การปรับปรุงเสถียรภาพทางความร้อนและการลดอันตรกิริยาระหว่างโพลิเมอร์/ $LiBH_4$ หลังการเติมมัลติวอลคาร์บอนนาโนทิวบ์ในการบรรจุระดับนาโนของ $LiBH_4$ ด้วยโพลีเมทิลเมตาคริเลต-โค-บิวทิลเมตาคริเลต

นางสาวประภัสสร เพลิดสระน้อย

IMPROVEMENT OF THERMAL STABILITY AND

REDUCTION OF POLYMER/LiBH₄ INTERACTION

AFTER MULTI-WALLED CARBON NANOTUBE

DOPING IN NANOCONFINED LiBH₄-POLY

(METHYL METHACRYLATE)-co-

BUTYL METHACRYLATE

Praphatsorn Plerdsranoy

A Thesis Submitted in Partial Fulfillment of the Requirements for the

Degree of Master of Science in Chemistry

Suranaree University of Technology

Academic Year 2013

IMPROVEMENT OF THERMAL STABILITY AND REDUCTION OF POLYMER/LiBH₄ INTERACTION AFTER MULTI-WALLED CARBON NANOTUBE DOPING IN NANOCONFINED LiBH₄-POLY (METHYL METHACRYLATE)-co-BUTYL METHACRYLATE

Suranaree University of Technology has approved this thesis submitted in partial fulfillment of the requirements for a Master's Degree.

Thesis Examining Committee

_____

(Assoc. Prof. Dr. Jatuporn Wittayakun)

Chairperson

_____

(Asst. Prof. Dr. Rapee Gosalawit-Utke)

Member (Thesis Advisor)

_____

(Asst. Prof. Dr. Kunwadee Rangsriwatananon)

Member

_____

(Asst. Prof. Dr. Sanchai Prayoonpokarach)

Member

_____   _____

(Prof. Dr. Sukit Limpijumnong)   (Assoc. Prof. Dr. Prapun Manyum)

Vice Rector for Academic Affairs   Dean of Institute of Science

and Innovation

ประภัสสร เพลิดสระน้อย : การปรับปรุงเสถียรภาพทางความร้อนและการลดอันตรกิริยา
ระหว่างโพลิเมอร์/LiBH$_4$ หลังการเติมมัลติวอลคาร์บอนนาโนทิวบ์ในการบรรจุระดับ
นาโนของ LiBH$_4$ ด้วยโพลีเมทิลเมตาคริเลต-โค-บิวทิลเมตาคริเลต (IMPROVEMENT OF
THERMAL STABILITY AND REDUCTION OF POLYMER/LiBH$_4$ INTERACTION
AFTER MULTI-WALLED CARBON NANOTUBE DOPING IN NANOCONFINED
LiBH$_4$-POLY (METHYL METHACRYLATE)-co-BUTYL METHACRYLATE.)
อาจารย์ที่ปรึกษา : ผู้ช่วยศาสตราจารย์ ดร.ระพี โกศัลวิตร-อูทเคอ. 62 หน้า.

คอมโพสิท/ เสถียรภาพทางความร้อน/ อันตรกิริยาระหว่างโพลิเมอร์และลิเทียมโบโรไฮไดร์

ในวิทยานิพนธ์นี้ การบรรจุระดับนาโนของ LiBH$_4$ ในโพลีเมทิลเมตาคริเลต-โค-บิวทิล
เมตาคริเลต (PcB) ที่คอมโพสิทกับมัลติวอลคาร์บอนนาโนทิวบ์ (MWCNT) ซึ่งใช้ชื่อเรียกตัวอย่างเป็น
นาโน LiBH$_4$–PcB–MWCNT ถูกตั้งสมมติฐาน ไม่เพียงแต่ด้านการปรับปรุงเสถียรภาพทางความ
ร้อนของโพลิเมอร์ โฮสต์ยังรวมถึงด้านการลดอันตรกิริยาระหว่าง LiBH$_4$/PcB ซึ่งจากเปรียบเทียบ
กับตัวอย่างที่ไม่ได้เติม MWCNT เสถียรภาพทางความร้อนของพอลิเมอร์เพิ่มขึ้นอย่างมีนัยสำคัญ
เมื่อเติม MWCNT ลงในตัวอย่าง เช่น ปริมาณโดยรวมของก๊าซที่ปล่อยเนื่องจากการสลายตัวด้วย
ความร้อนของ PCB ในตัวอย่างบรรจุระดับนาโนลดลง 86% หลังจากเติม MWCNT เพียง 0.1% โดย
น้ำหนัก การลดอันตรกิริยาระหว่าง LiBH$_4$/PcB ถูกยืนยันโดยอัตราส่วนระหว่างพื้นที่ใต้พีคของพีค
การสั่นแบบยืดของพันธะ B–H เทียบกับ พีคการสั่นแบบยืดของพันธะ C = O (υ(B–H) / υ(C = O))
จาก FT–IR สเปกตรัม โดยพบว่าตราส่วนของ υ(B–H) / υ(C = O) ของนาโน LiBH$_4$–PcB–
MWCNT มีค่าเพิ่มขึ้นอย่างมีนัยสำคัญถึง 78% สิ่งนี้สอดคล้องกันกับผลที่ได้ใน B 1s ของ XPS ที่
สัดส่วนระหว่างพีคของ B$_x$O$_y$ (x/y = 3) ต่อ LiBH$_4$ ลดลงหลังจากการเติม MWCNT สำหรับ
จลนพลศาสตร์การปลดปล่อยก๊าซ H$_2$ ของตัวอย่าง ปริมาณก๊าซ H$_2$ ที่ใกล้เคียงกันถูกได้รับจาก
ตัวอย่างบรรจุระดับนาโนทั้งสอง ในรอบที่ 1 คือ 6.7 และ 6.6% โดยน้ำหนักเมื่อเทียบกับปริมาณ
ของ LiBH$_4$ ในตัวอย่างจากนาโน LiBH$_4$–PCB และนาโน LiBH$_4$–PCB–MWCNT ตามลำดับ
จลนพลศาสตร์ที่ช้าถูกพบในนาโน LiBH$_4$–PCB–MWCNT อาจเนื่องมาจากการกระจายตัวอย่างไม่
เป็นระเบียบของ MWCNT ใน PCB ขัดขวางการแพร่กระจายของก๊าซ H$_2$ ในเนื้อโพลิเมอร์ หลังจาก
ปฏิกิริยาการเติมก๊าซ H$_2$ที่อุณหภูมิ 120 °C ภายใต้ความดันบรรยากาศก๊าซ H$_2$ ที่ 60 บาร์ พบว่า

นาโน $LiBH_4$–PCB–MWCNT แสดงปริมาณของก๊าซ H_2 ที่ปล่อยออกมาในรอบที่ 2 เป็น 37.3% เมื่อเทียบกับค่าความสามารถในการจัดเก็บตามทฤษฎี ซึ่งสูงกว่า นาโน $LiBH_4$–PCB (20.0%)

สาขาวิชาเคมี ลายมือชื่อนักศึกษา _____

ปีการศึกษา 2556 ลายมือชื่ออาจารย์ที่ปรึกษา _____
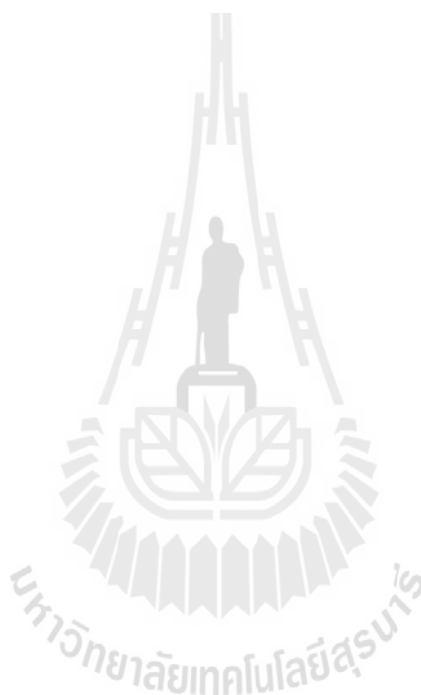
PRAPHATSORN PLERDSRANOY : IMPROVEMENT OF THERMAL
STABILITY AND REDUCTION OF POLYMER/LiBH$_4$ INTERACTION
AFTER MULTI-WALLED CARBON NANOTUBE DOPING IN
NANOCONFINED LiBH$_4$-POLY (METHYL METHACRYLATE)-co-BUTYL
METHACRYLATE. THESIS ADVISOR : ASST. PROF. RAPEE
GOSALAWIT–UTKE, Ph.D. 62 PP.

COMPOSITE/ THERMAL STABILITY/ POLYMER– LiBH$_4$ INTERACTION

In this thesis, nanoconfinement of LiBH$_4$ in poly (methyl methacrylate)-co-
butyl methacrylate (PcB) compositing with multi-walled carbon nanotube (MWCNT),
denoted as nano LiBH$_4$–PcB–MWCNT, was hypothesized not only to improve thermal
stability of polymer host, but also to reduce LiBH$_4$/PcB interaction. As compared to
nanoconfined sample without MWCNT, thermal stability of polymer matrix was
significantly improved by MWCNT addition, for example, the total amount of gases
release due to thermal degradation from PcB in nanoconfined samples reduces by 86%
after doping with 0.1 wt. % of MWCNT. The reduction of LiBH$_4$/PcB interaction is
confirmed by the ratio of B–H stretching peak area with respect to that of C=O
stretching (υ(B–H)/υ(C=O)) of FT–IR spectra. It is found that υ(B–H)/υ(C=O) ratio
significantly increases up to 78%. This is in agreement with B 1s XPS results, where
the relative amount of B$_x$O$_y$ (x/y=3) to LiBH$_4$ decreases after MWCNT doping. For
dehydrogenation kinetics, comparable amounts of H$_2$ released were obtained from both
nanoconfined samples in the 1st cycle, i.e., 6.7 and 6.6 wt. % H$_2$ with respect to LiBH$_4$
content from nano LiBH$_4$–PcB and nano LiBH$_4$–PcB–MWCNT, respectively. The slow
kinetics observed in nano LiBH$_4$–PcB–MWCNT might be due to the random dispersion
of MWCNT in PcB hindering the diffusion of H$_2$ in the polymer matrix. After

rehydrogenation at 120 °C under 60 bar H_2, nano $LiBH_4$–PcB–MWCNT exhibits the amount of hydrogen reproducibility in the 2nd cycle of 37.3% with respect to theoretical hydrogen capacity, which is higher than that of nano $LiBH_4$–PcB (20.0%).

School of Chemistry   Student's Signature_____

Academic Year 2013   Advisor's Signature _____

ACKNOWLEDGEMENT

CONTENTS

CONTENTS (Continued)

CONTENTS (Continued)

LIST OF TABLES

LIST OF FIGURES

LIST OF FIGURES (Continued)

CHAPTER I

INTRODUCTION

1.1 Hydrogen energy

With global warming and decrease of fossil fuel, several attempts to investigate an alternative clean and renewable energy are of interest. Hydrogen has attracted a great deal of attention as a clean fuel for mobile and stationary applications because it can be used in a fuel cell, producing energy free of any pollutant by–products. Hydrogen can be produced in a sustainable way from water using solar, wind, nuclear energy, and also from biomass. The replacement of gasoline fuelled combustion engines for transportation with hydrogen fuel cell vehicles will significantly reduce both oil demand and air pollution. Hydrogen-fuel cell cars are currently the focus of intense research and development activity worldwide and are expected to reach commercial applications in 2015 (Tollefson, 2010).

Figure 1.1 shows a typical hydrogen cycle consisting of three major steps, which are hydrogen production from renewable energy sources (solar), storage of hydrogen, and its use in fuel cell to produce energy. Each of these steps is associated with significant technical challenges that must be solved before the benefits of using hydrogen as an energy carrier can be fully realized.
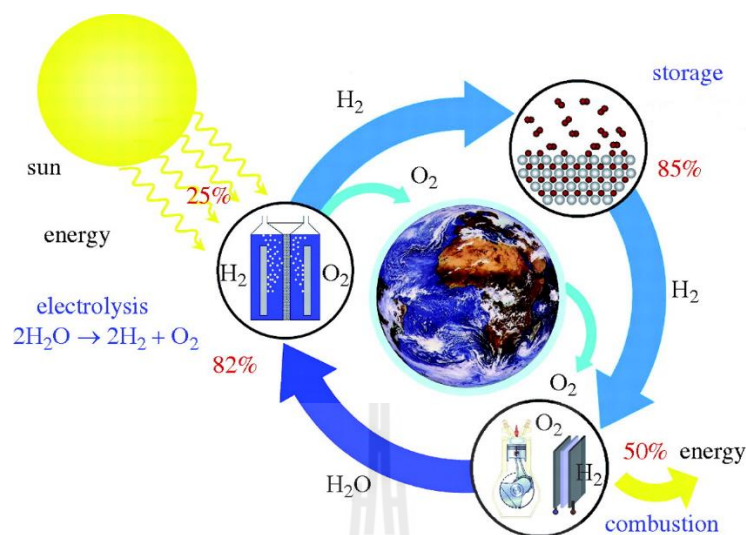
Figure 1.1 Hydrogen cycle (Züttel et al., 2008).

The energy from sunlight is converted into electricity by solar cells. The electricity is used to split water into hydrogen and oxygen. The oxygen is released in the atmosphere while the hydrogen is transported, stored, and distributed to fuel cell. Finally, hydrogen and oxygen from air are reacted electrochemically in a fuel cell to produce electricity and heat giving water as the by product (Figure 1.1).

1.2 Hydrogen fuel cells

Fuel cells are promising technology for use as a source of heat and electricity for buildings, and as an electrical power source for electric motors propelling vehicles. A proton exchange membrane fuel cell (PEMFC) is an electrochemical cell that is fed with hydrogen, which is oxidized at the anode, and oxygen that is reduced at the cathode. The protons released during the oxidation of hydrogen are conducted through the proton exchange membrane to the cathode. Since the membrane is not electrically conductive, the electrons released from hydrogen travel to the electrical circuit and an electrical current is

generated. These reactions and pathways are shown schematically in Figure 1.2.
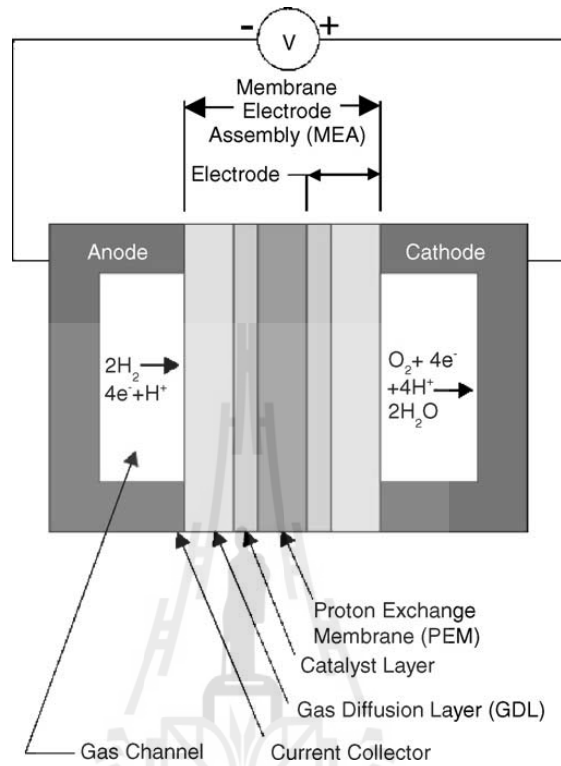
Figure 1.2 Schematic draw of a single proton exchange membrane fuel cell (Litster and McLean, 2004).

The PEM fuel cell is consisted of gas diffusion layer (GDL), catalyst layers, and proton exchange membrane. The membrane electrode assembly (MEA) is typically sandwiched by two flow field plates that are often mirrored to make a bipolar plate when cells are stacked in series for greater voltages. Typically, these components are fabricated individually and then pressed together at high temperatures and pressures (Litster and McLean, 2004). From Figure 1.2, the hydrogen gas flows to the anode and dissociate to proton and electron:

$$2H_2 \longrightarrow 4H^+ + 4e^- \tag{1}$$
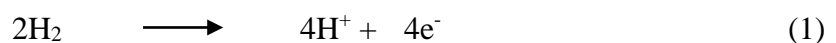
Afterwards, protons pass through the membrane to the cathode, while electrons

travel through an external circuit to the cathode. The flow of electrons through this circuit creates the electricity. Oxygen gas, usually drawn from the outside air, flows to the cathode and react with proton and electron to form water as this reaction:

$$O_2 + 4H^+ + 4e^- \longrightarrow 2H_2O + \text{Heat} \tag{2}$$

Overall reaction:

$$2H_2 + O_2 \longrightarrow 2H_2O + \text{Heat} \tag{3}$$
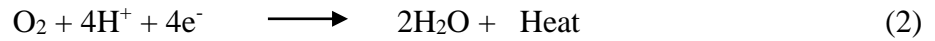
The potential power generated by a fuel cell stack depends on the number and size of the individual fuel cell that comprise the stack and the surface area of the PEM. Therefore, to run fuel cell stacks efficiently, hydrogen storage materials with high capacity is required.

1.3 Hydrogen storage

Another crucial challenge facing the wide spread use of hydrogen as a fuel especially for mobile applications is how to store hydrogen on-board in an efficient, safe and cost effective way (Schlapbach and Züttel, 2001). For hydrogen storage systems, current options include storing hydrogen in its liquid form, as a compressed gas, and solid–state hydrogen storage. The comparison of three major competing technologies for hydrogen storage is shown in Table 1.

Table 1 Comparison of three major competing technologies for hydrogen storage. (Varin et al., 2009)

Storage systems	Volumetric hydrogen capacity $(kgH_2 \text{ m}^{-3})$	Drawbacks
Compressed hydrogen gas under pressure 80 MPa	36.0	Safety problem due to enormous pressures; cost of pressurization; large pressure drop during use; hydrogen embrittlement of storage tanks
Liquid hydrogen at cryogenic tank at 21 K (-252 °C)	70.8	Large thermal losses (open system); safety; cost of liquefaction
Solid–state hydrides	80.0 – 160.0	None of the above

Liquid hydrogen is stored in cryogenic tanks at 21.2 K and ambient pressure. Because of the low critical temperature of hydrogen (33 K), liquid hydrogen can only be stored in a closed system. The volumetric density of liquid hydrogen is 70.8 kg m^{-3}. This system has major drawbacks such as a big cost of liquefaction, safety issues associated with the handling of cryogenic liquids and the problem of evaporative loss (Varin et al., 2009).

For compressed gas storage, high pressure gas cylinders have a maximum pressure of 20 MPa. New light weight composite cylinders have been developed and they can support pressure up to 80 MPa. Hydrogen reaches a volumetric density of 36 kg m^{-3}, approximately half as much as in its liquid state (Züttel et al., 2003). The safety of pressurized cylinders is an important issue of concern. Furthermore, the cost of compression and large pressure drop during use are considered as the main obstacles for practical uses of this system. In addition, because most of the system parts exposed to hydrogen are metallic, hydrogen embrittlement of storage tanks is also a concern.

The highest volumetric densities of hydrogen are found in solid–state hydrogen

storages. The use of solid absorbers such as metallic hydrides is intrinsically safe and has a volumetric capacity (80–160 kg m^{-3}) higher than liquid hydrogen and compressed gas. However, the gravimetric capacity, i.e. the weight of the stored hydrogen related to that of retaining material, is low. Moreover, it is necessary to have materials that can easily release and uptake hydrogen under acceptable pressure and temperature conditions. On the basis of solid state hydrogen storage, hydrogen can be stored in following two different routes. The first one is based on the chemical absorption of atomic hydrogen in simple or complex light metallic hydrides, while the second one relies on the adsorption of molecular hydrogen on high surface area materials (Principi et al., 2009).

The American Department of Energy (DOE) presented several requirements for an on-board hydrogen storage system. To obtain an easy and safe system, a low operating temperature and pressure system is desired. The requirements for effective on-board hydrogen storage are:

i)   favorable thermodynamics of hydrogen absorption and desorption,

ii)   fast re/dehydrogenation kinetics,

iii)   high storage capacity ($\geq$ 9 wt. %H$_2$ by 2015),

iv)   effective heat transfer,

v)   high volumetric densities,

vi)   long cycle lifetime for hydrogen absorption/desorption,

vii)   high mechanical strength and durability,

viii) high safety under the conditions used,

ix)   cheap components and materials.

According to the US–DOE targets for a hydrogen storage system, several research groups have focused on the solid–state hydrides, due to their high hydrogen storage

capacity. Nevertheless, there are still a lot of barriers that need to be overcome, because almost metallic or complex hydrides have high hydrogen de/absorption temperatures and poor kinetics of hydrogen exchange reactions. Moreover, some of them can release toxic gases during the dehydrogenation process. Therefore, the development of solid–state hydrides for on– board application is still in progress.

CHAPTER II

LITERATURE REVIEW

2.1 Lithium borohydride (LiBH₄)

Among various solid–state hydrogen storage materials (e.g., metal hydrides, complex metal hydrides, nanocarbon materials, and metal organic frame–works), lithium borohydride ($LiBH_4$) is one of the most attractive complex hydrides for reversible hydrogen storage, due to its high hydrogen storage capacity and hydrogen density of 18.5 wt. % H_2 and 121 kg H_2 m^{-3}, respectively. The structure of $LiBH_4$ is orthorhombic at room temperature (Harris et al., 1947). Each $[BH_4]^-$ anion is surrounded by four Li^+ cations and vice versa for Li^+, where both ions are in tetrahedral configurations (Li et al., 2011) (Figure 2.1).
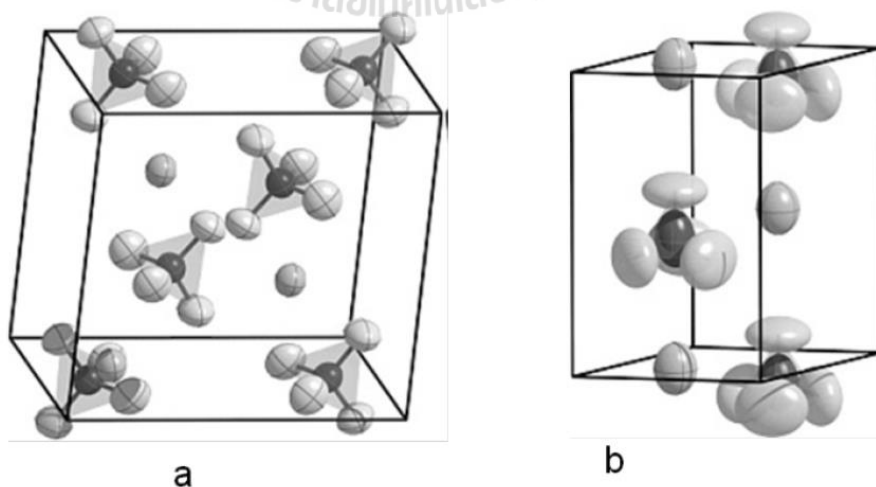
Figure 2.1 Crystal structure of LiBH₄ phases (a) orthorhombic and (b) hexagonal (Ngene, 2012).

For decomposition process of $LiBH_4$, the phase transition of $LiBH_4$ from the low temperature phase (orthorhombic structure) to the high temperature phase (hexagonal structure) was observed at a temperature around 110 °C (Figure 2.1). $LiBH_4$ melts at 280 °C and releases hydrogen in the melted state in two steps as shown in the following equations:

$$2LiBH_4 \longrightarrow 2LiH + 2B + 3H_2 \tag{1}$$
$$2LiH \longrightarrow 2Li + H_2 \tag{2}$$
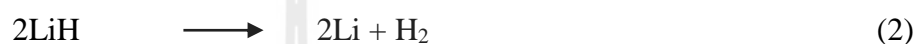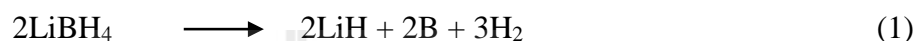
At low temperature (100– 200 °C), only 0.3 wt. % H_2 is released. In the temperature range of 320–380 °C, 13.6 wt. % H_2 is theoretically released, corresponding to reaction (1), while 4.5 wt. % H_2 remain in the form of LiH. The latter requires up to 600 °C to complete dehydrogenation, as shown in reaction (2) (Züttel et al., 2003). Generally, only reaction (1) is considered as dehydrogenation process of $LiBH_4$ because reaction (2) requires too high desorption temperature. Furthermore, an alternative dehydrogenation pathway through the formation of $Li_2B_{12}H_{12}$ intermediate (reaction (3)) has been proposed (Ozolins et al., 2009, Orimo et al., 2006, Friedrichs et al., 2010).

$$12LiBH_4 \longrightarrow Li_2B_{12}H_{12} + 10LiH + 13H_2 \tag{3}$$
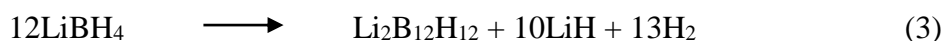
Reaction (3) can theoretically result in 10 wt. % H_2. Recently, Friedrichs et al. (2010) have reported that $Li_2B_{12}H_{12}$ was formed through the reaction between B_2H_6, derived from the thermal decomposition of $LiBH_4$ and the remaining un-decomposed $LiBH_4$ during the dehydrogenation process. However, $Li_2B_{12}H_{12}$ is an undesirable phase because it causes the reduction of hydrogen content released from $LiBH_4$. For rehydrogenation, dehydrogenated products from reaction (1) can absorb H_2 to form $LiBH_4$ as shown in reaction (4).

$$2LiH + 2B + 3H_2 \longrightarrow 2LiBH_4 \tag{4}$$

In principle, it is possible, but a rigorous condition (T = 690 °C, P (H$_2$) = 200 MPa H$_2$, 12 h.) is required to complete the rehydrogenation (Orimo et al., 2005). Therefore, to improve the de/rehydrogenation properties of LiBH$_4$, several approaches have been investigated.

2.2 Modification of LiBH$_4$

2.2.1 Catalytic doping

The first method deals with catalytic doping. Züttle et al. (2003) indicated that desorption temperature of LiBH$_4$ could be lowered to 100 °C with the main hydrogen desorption around 200 °C by adding SiO$_2$–powder (25 wt. %). However, there was an undesired effect from addition of SiO$_2$, i.e. the formation of diborane (B$_2$H$_6$) during the dehydrogenation process, which can damage downstream systems like fuel cells. Moreover, some additives, such as metals (Mg and Al) (Yang et al., 2007), transition metals (Ni and Au) (Xia et al., 2009), oxides (SiO$_2$, Fe$_2$O$_3$, TiO$_2$, etc.) (Yu et al., 2009), and halides (TiCl$_3$, MgCl$_2$, NiCl$_2$, etc.) (Au et al., 2008), were effective in reducing dehydrogenation temperature of LiBH$_4$.

Pendolino et al. (2009) studied the decomposition kinetics of LiBH$_4$ with and without boron additive under various hydrogen pressures. It was found that the addition of boron reduced the dehydrogenation temperature and activation energy (E$_a$) of LiBH$_4$ from 500 to 350 °C and from 59 ± 2 to 54.8 ± 0.7 kJ/ mol, respectively. Concurrently, the sample of LiBH$_4$–Ni was reported to release the majority of hydrogen below 600 °C together with complete rehydrogenation at 600 °C under 10 MPa H$_2$ (Xia et al., 2009). Yu et al. (2008) investigated the hydrogen desorption properties of LiBH$_4$ ball–milled with TiO$_2$. With respect to the mass ratio of 4:1 (LiBH$_4$: TiO$_2$), the onset temperature for LiBH$_4$

dehydrogenation reduced to 150 °C. It was declared that the destabilization of borohydride, achieved via a redox reaction with the TiO_2 to form $LiTiO_2$, liberated all available hydrogen from $LiBH_4$. Furthermore, $LiTiO_2$ could accelerate the decomposition of $LiBH_4$ via the formation of Li_2O and TiB_2, resulting in a total hydrogen release of 9.0 wt. % H_2. Afterward, the effect of other metal oxides on the dehydrogenation of $LiBH_4$ was further studied. X–ray diffraction revealed that the destabilization of $LiBH_4$ is obtained via the redox reaction with metal oxides as in the following reaction:

$$LiBH_4 + MO_x \longrightarrow LiMO_x + B + 2H_2 \tag{5}$$
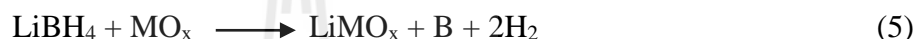
The order of destabilization effect of metal oxides on $LiBH_4$ was $Fe_2O_3 > V_2O_5 > Nb_2O_5 > TiO_2 > SiO_2$. It should be noted that milled $LiBH_4$–Fe_2O_3 sample (mass ratio of 1:2 ($LiBH_4$:Fe_2O_3)) released 6 wt. % H_2 at temperature below 200 °C (Yu et al., 2009).

In addition, several metal halides, such as $TiCl_3$, TiF_3, and ZnF_2 have been of interest to destabilize $LiBH_4$ based on cation exchange interaction, while some of them (MgF_2, $MgCl_2$, $CaCl_2$, $SrCl_2$, and $FeCl_3$) did not function properly (Au et al., 2008). Milled $LiBH_4$ –TiF_3 (mole ratio of 3:1) started to release hydrogen at approximately 100 °C, and reached the storage capacity of 5.0 wt. % H_2 at 250 °C (Guo et al., 2010). The mechanochemical process of $4LiBH_4 + VCl_n$ mixtures (with n = 2 and 3) produced crystalline LiCl and excess $LiBH_4$. The reactions with VCl_3 had stronger thermodynamical driving forces than with VCl_2 (Llamas–Jansa et al., 2011). $LiBH_4$ that was significantly destabilized by addition of $FeCl_2$, $CoCl_2$ and $NiCl_2$ could perform the main dehydrogenation in the temperature range of 230 °C to 300 °C, resulting in major hydrogen desorption. It is important to mention that the addition of $FeCl_2$ and $NiCl_2$ resulted in complete hydrogen desorption of $LiBH_4$, but $CoCl_2$ yielded the formation of a small amount of B_2H_6 (Zhang et al., 2010). Moreover, it was reported that ball milling of $LiBH_4$

with chloride of Ce and La produced $Ce(BH_4)_3$ and $La(BH_4)_3$, while fluoride of Ce and La did not react with $LiBH_4$ during ball milling at room temperature. The ball milled mixtures demonstrated dehydrogenation temperatures around $220 - 320\,°C$, which were much lower than that of pure $LiBH_4$ (Zhang et al., 2010).

2.2.2 Composite materials

Not only metal halides and oxides were commonly used as additives in $LiBH_4$ systems, but also metal hydrides and complex hydrides were regularly milled with $LiBH_4$ to form reactive hydride composites (RCHs). One of the typical $LiBH_4$–RHCs is $2LiBH_4$–MgH_2. On the basis of the $2LiBH_4$–MgH_2 dehydrogenation reaction (reaction (6)), the formation of MgB_2 reduced the de/rehydrogenation enthalpy by 25 kJ/ (mol H_2) at $400\,°C$ as compared with pure $LiBH_4$ (Vajo et al., 2005).

$$2LiBH_4 + MgH_2 \quad \longleftrightarrow \quad 2LiH + MgB_2 + 4H_2 \qquad (6)$$

The theoretical hydrogen capacity of reaction (6) is 11.4 wt. % H_2. In addition, $LiBH_4$ can be modified by ball–milling with Al or Al containing compounds (Kang et al., 2007, Mao et al., 2009, Ravnsbaek et al., 2010). Kang et al. (2007) found that the $LiBH_4$–Al system possessed a theoretical capacity of 8.5 wt. % H_2, and it could be reversible at temperature between $400–450\,°C$. During cycling, AlB_2 was formed in the dehydrogenated state and disappeared in the hydrogenated state. This compound increases the stability of the products, resulting in a lower desorption temperature of this system.

The composite of $6LiBH_4$–CaH_2 has recently received much attention, as it can store a large amount of hydrogen (11.7 wt. % H_2) through the following reaction (7) (Ibikunle et al., 2009, Lim et al., 2010, Pinkerton et al., 2008):

$$6LiBH_4 + CaH_2 \quad \longleftrightarrow \quad 6LiH + CaB_6 + 10H_2 \qquad (7)$$
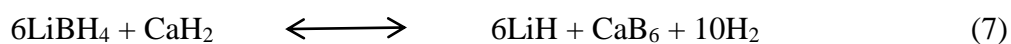
The dehydrogenation reaction enthalpy of reaction (7) was in the range of 40.7–60.2 kJ/mol H_2 (Pinkerton et al., 2008). Moreover, $LiBH_4$ could be destabilized by mixing with $LiNH_2$ (2:1 molar ratio) and the mixture desorbed a large amount of hydrogen (11.9 wt. % H_2) at temperatures above 250 °C. However, it was found that not only hydrogen was released as a product of this composite, but also a small amount of undesirable NH_3 was formed simultaneously with H_2 release (Pinkerton et al., 2005). From the catalytic doping and composite materials, solid-state hydrides are agglomerated when they were used for several cycles. The agglomeration of hydride particles reduces the diffusion rate of hydrogen gas, resulting in the reduction of the volumetric capacity of system (Figure 2.2).
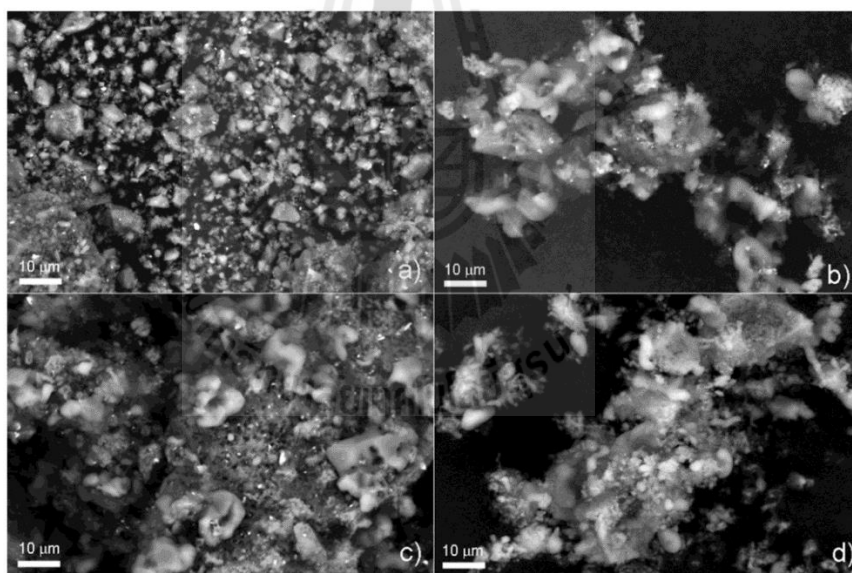
Figure 2.2 SEM-BSE images of 5 wt. % Fe-doped MgH_2, ball milled for 10 h, after (a) 1st cycle; (b) 22th cycles and (c) 47th cycles at 300 °C; (d) SEM-BSE images of pure MgH_2, ball milled for 10 h after 22th cycles, at 350 °C. (Montone et al., 2012)

2.2.3 Confinement in nanoporous hosts

With respect to the shorter diffusion distances between hydrogen molecules and the other light elements within a nanoscale structure, resulting in faster de/ rehydrogenation

rates (Gross et al., 2008), the third method to destabilize LiBH$_4$ by confining LiBH$_4$ in nanoporous materials has been recently addressed. Ngene et al. (2010) prepared LiBH$_4$/SBA−15 by melt infiltration under hydrogen pressure. The result showed that mesopores of SBA−15 was successfully filled with LiBH$_4$, and that the long−range order of the mesopores was maintained. The dehydriding temperature of nanoconfined LiBH$_4$ was considerably reduced to 150 °C. However, reaction between SiO$_2$ and LiBH$_4$ during decomposition with formation of undesirable phases of Li$_2$SiO$_3$ and Li$_4$SiO$_4$ led to irreversibility in the next cycle due to Li loss. In addition, Sun et al. (2012) reported that the composite of LiBH$_4$/SBA−15 prepared by solution impregnation revealed remarkable onset dehydrogenation temperature at 45 °C together with 8.5 wt. % H$_2$ within 10 min at 105 °C. Nevertheless, this system was also irreversible.

Due to the unwanted reaction between SiO$_2$ and LiBH$_4$, inert carbon host materials with nanoporous structures were introduced. Gross et al. (2008) demonstrated that the carbon aerogel scaffold (CAS) served not only as a nanoscale structure−directing agent, but also as a host medium for preventing particle growth during cycling. It was shown that the dehydrogenation rate was improved considerably due to nanoconfinement in CAS, for example, LiBH$_4$ nanoconfined in CAS with 13 nm pore size could reach up to 50 times faster dehydrogenation kinetics at 300 °C with respect to bulk LiBH$_4$. Furthermore, the effects of pore size from various types of CAS on LiBH$_4$ desorption have been investigated. Calorimetry signals of both structural phase transition (from o−LiBH$_4$ to h−LiBH$_4$) and melting (h−LiBH$_4$) of nanoconfined LiBH$_4$ shifted to a lower temperature with respect to the bulk material, and they finally disappeared with the pore size less than 4 nm due to the amorphous state of LiBH$_4$. Moreover, the reduction in the dehydrogenation temperature and the lack of B$_2$H$_6$ formation were achieved when the pore size of CAS decreased (Liu

et al., 2011). The melting and decomposition behavior of LiBH$_4$ has been investigated in the presence of highly ordered nanoporous hard carbon (NPC) with hexagonally packed 2 nm diameter columnar pores. The onset desorption temperature of premelted LiBH$_4$–NPC was reduced from 460 to 220 °C. The signal of B$_2$H$_6$ during dehydrogenation was detected in bulk LiBH$_4$ and physical mixtures of LiBH$_4$–NPC, while that of pre–melted LiBH$_4$– NPC was negative. These results illustrated that the nanoframework altered the decomposition pathway and eliminated the formation of B$_2$H$_6$ (Liu et al., 2010). Fang et al. (2008) reported that the dehydrogenation temperature of LiBH$_4$ incorporated into activated carbon (AC) was lowered by 150 °C as compared with bulk LiBH$_4$. The dehydrogenation rate was increased by over one order of magnitude. Moreover, the temperature and hydrogen pressure required for rehydrogenation were significantly reduced. The nanoconfinement of metal hydrides in nanoporous hosts is an effective method to destabilize LiBH$_4$. However, temperature and hydrogen pressure required for de/rehydrogenation of nanoconfined materials were still significantly high

2.3 Metal hydride polymer composites

The use of polymeric materials as an embedding matrix for hydride materials was also reported. Pentimalli et al. (2009) reported the impregnation of active metal particles in polymeric host. A ball milling in tumbling mode was used to prepare the composite of LaNi$_5$–ABS with a high metal to powder weight ratio. The composite was further consolidated by hot pressing and the pellets were characterized in term of their hydriding– dehydriding properties. The materials did not the significant losses neither in loading capacity nor kinetic properties as compared with the hydride material. It should be noted that the polymeric host was stable along hydrogen release and uptake cycles. Furthermore,

SEM images confirmed that the metal particles were still embedded in the polymeric matrix even after a number of cycles as well as the overall dimensional integrity was retained (Figure 2.3).
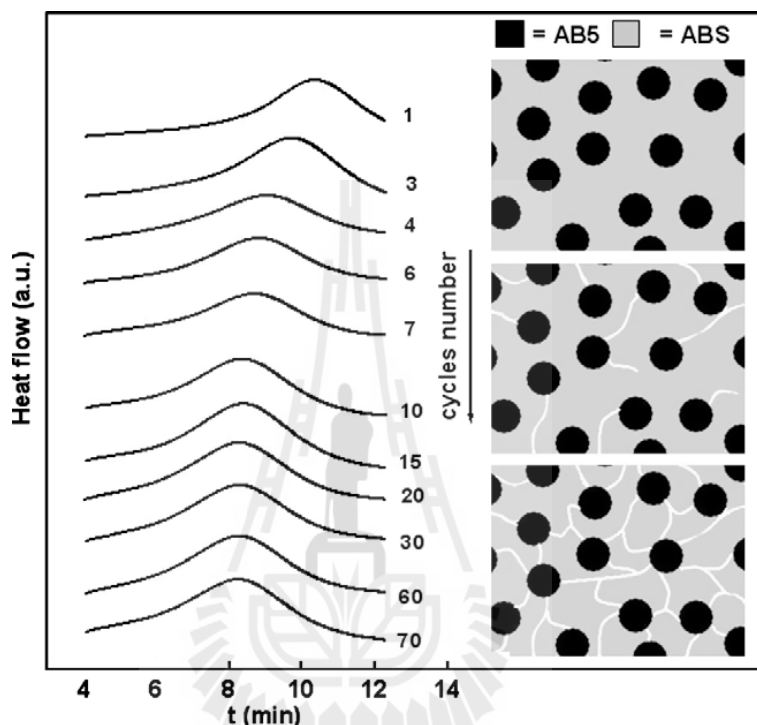
Figure 2.3 H_2 desorption curves obtained by HP-DSC experiments of LaNi5-ABS pellet consolidated at 175 °C (left side panel) and schematic representation of the consolidated composite material evolution as a function of the cycling number (right side panel) (Pentimalli et al., 2009).

Checchetto et al. (2009) studied the hydrogen storage capacity and sorption kinetics of composite materials made of metal and alloy particles (Pd and LaNi$_5$, particle size of ~1 µm) embedded into hydrogen permeable polymers such as polysiloxane (PS), polyethylene (PE), and polyvinylpyrolidone (PVP). No interaction between an activated metal surface and polymeric chain was observed. The slow kinetics of the composite could be explained by time comsumtion due to the H_2 diffusion process into the polymeric part of the

composites. Moreover, the agglomeration of metal particles in polymer matrix were detected (Figure 2.4)
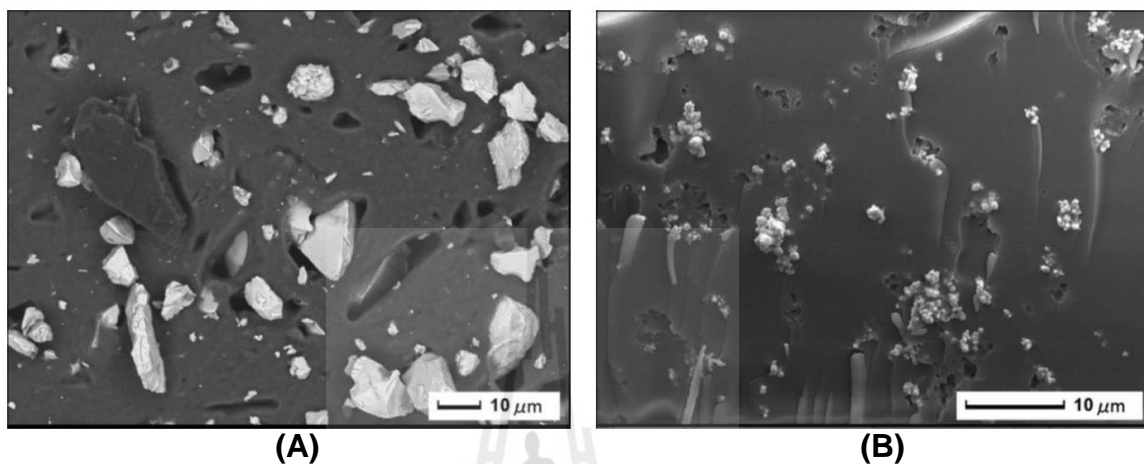
Figure 2.4 SEM micrographs of as prepared PS−LaNi5 (A) and PVP−Pd (B) composites (Checchetto et al., 2009).

Furthermore, Poly methyl methacrylate (PMMA) proposed as one of the hydrogen permeable polymers with a high permeability ratio of H_2/O_2 (H_2/O_2 permeability ratio of 42.9 at 35 °C) was composited with metallic Mg nanocrystals (NCs) (Jeon et al., 2011). The PMMA−NCs composite enabled both the storage of a high capacity of H_2 (up to 6 wt. % H_2 at 200 °C) and rapid kinetics without using expensive heavy−metal catalysts (Figure 2.5).
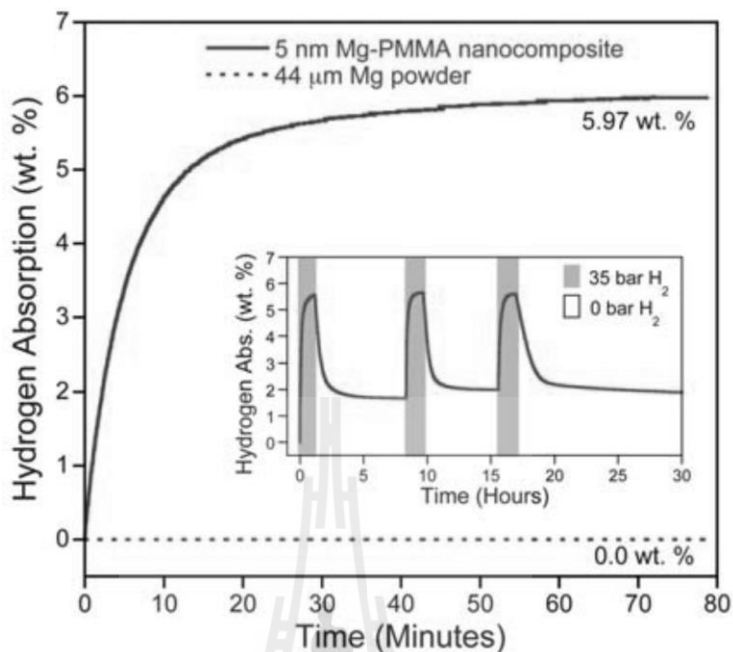
Figure 2.5 Hydrogen absorption curve at 200 °C and 35 bar H_2 of Mg-PMMA nanocomposite and hydrogen absorption/desorption cycling of the nanocomposites at 200 °C (inset) (Jeon et al., 2011).

Due to high hydrogen permeability of PMMA, in which hydrogen could diffuse in and out freely (Figure 2.6), the nanoconfinement of $LiBH_4$ in PMMA pore network structure led to fast hydrogen release from $LiBH_4$ at low temperature ($\Delta T = 237$ °C as compared with pure $LiBH_4$) (Huang et al., 2014). In addition, polymer host of PMMA providing hydrophobic properties can prevent $LiBH_4$ deterioration due to oxidation in ambient condition.
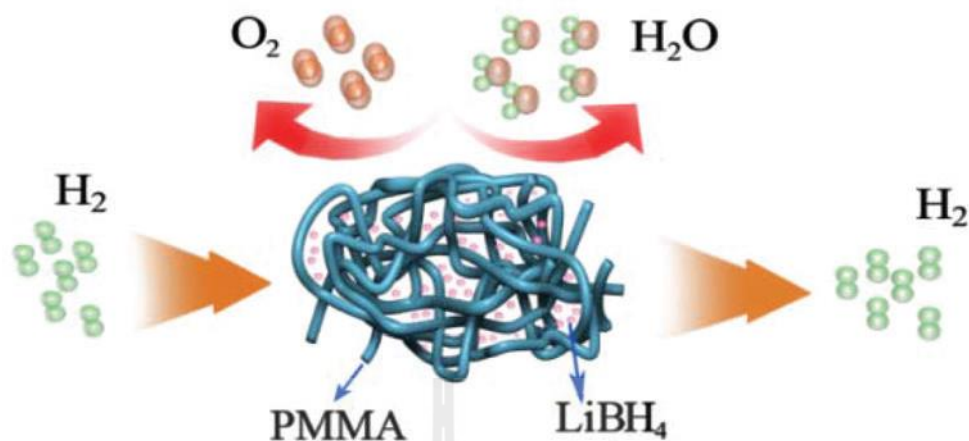
Figure 2.6 Schematic illustration of LiBH$_4$ protected from oxygen and water by PMMA (Huang et al., 2014).

Recently, Gosalawit-Utke et al. (2014) reported nanoconfined LiBH$_4$ in a new host material of poly (methyl methacrylate) –co–butyl methacrylate (PMMA–co–BM), denoted as nano LiBH$_4$–PMMA–co–BM. Long butyl branches of PMMA–co–BM providing superior amorphous degree and free volume to PMMA could benefit hydrogen permeability. The results indicated that the nanoconfined sample started to release hydrogen at ~80 °C and released up to 8.8 wt. % H$_2$ with respect to LiBH$_4$ content within 4 h at 120 °C under vacuum. Moreover, the nano LiBH$_4$–PMMA–co–BM can be rehydrogenated under considerably mild conditions of $T = 140$ °C and $P(\text{H}_2) = 50$ bar. However, the interaction between LiBH$_4$ and pendant group of PMMA–co–BM led to the reduction of hydrogen storage capacity. Also, the gas analysis results revealed that not only hydrogen released from nano LiBH$_4$–PMMA–co–BM, but also the gaseous products (CO, CO$_2$, •CH$_3$, and •OCH$_3$) from thermal degradation of polymer matrix were detected.

In the this work, we intend to solve the problems of nano LiBH$_4$–PMMA–co–BM; that is, (i) to improve thermal stability of PMMA–co–BM host and (ii) to reduce the interaction between LiBH$_4$ and PMMA–co–BM. Therefore, an idea of polymer composite

prepared from PMMA–co–BM and multi–walled carbon nanotube (MWCNT) for LiBH$_4$ embedding is of interest.

2.4 Polymer/ Multi-walled carbon nanotube composite

Carbon nanotubes is well known as a material providing an excellent thermal conductivity and good thermal stability, while most polymers exhibit a rather poor thermal conductivity and degrade under the effect of temperature (Chipara et al., 2013). The loading of polymeric matrices with carbon nanotubes usually increases the thermal conductivity of the matrix, resulting typically in the enhancement of the thermal stability of the polymer matrix (Chipara et al., 2009).

It was reported that the addition of multi-walled carbon nanotube (MWCNT) could increase the glass transition (T_g), melting (T_m) and decomposition temperature (T_d) of polymer matrix due to their constraint effect on the polymer segments and chains (Swain et al., 2010). Kashiwaki et al. (2002) reported that the decomposition temperature of poly (propylene) (PP) was significantly enhanced by 12 °C when compositing with 2 vol. % of MWCNT (Figure 2.7).
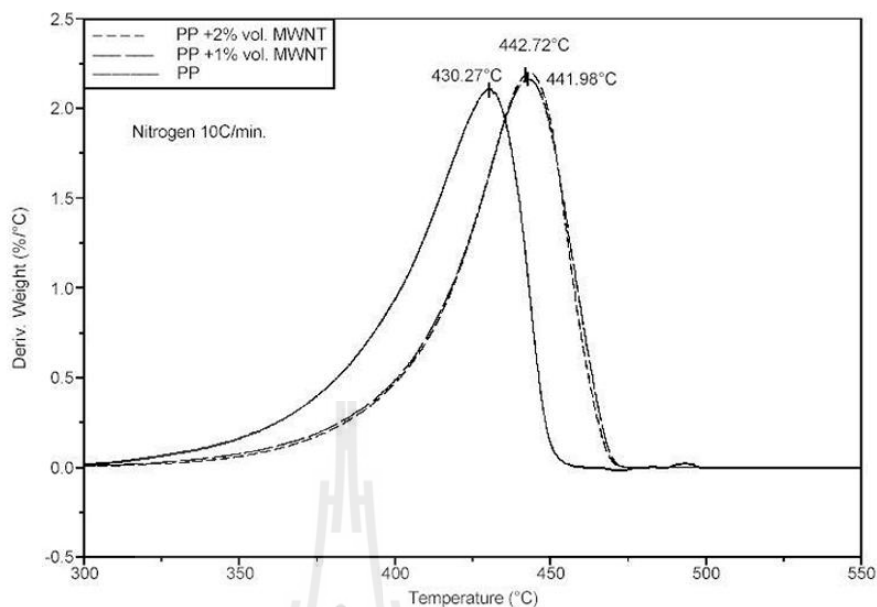
Figure 2.7 TGA analyses of normalized mass loss rate by the initial sample mass at a heating rate of 10 °C/min in nitrogen atmosphere (Kashiwagki et al., 2002).

The uniform dispersion and interaction between polymer matrix and carbon nanotube play the key role on the properties (i.e. mechanical strength, conductivity, thermal stability, and etc.) of composite (Swain et al., 2010). There are three main mechanisms of interaction of polymer matrix with carbon nanotubes (Bal and Samal, 2007):

(i) **Micro-mechanical interlocking** – Local non-uniformity along a CNT, including varying diameter and bends/kinks at places as a result of non-hexagonal defects, contribute to CNT-polymer adhesion by mechanical interlocking.

(ii) **Chemical bonding between the nanotubes and the matrix** – This improves interfacial interaction through ionic or covalent bond that enables a stress transfer.

(iii) **Weak van der waals bonding between the CNT and matrix** – Under no chemical bonding between CNT-polymer, the origins of CNT-polymer interactions are electrostatic and van der waals forces.

To avoid the agglomeration of MWCNT in polymer matrix and to compromise the thermal stability, hydrogen permeability, and hydrogen storage capacity, in this work only 0.1 wt. % of MWCNT was added to nano LiBH$_4$–PMMA–co-BM system.

2.5 Research objectives

2.5.1 To prepare nonoconfined LiBH$_4$ in PMMA–co–BM–MWCNT composite.

2.5.2 To improve thermal stability of PMMA–co–BM and reduce the interaction between LiBH$_4$ and PMMA–co–BM.

2.5.3 To study hydrogen storage properties, reversibility, and reaction mechanisms during de/rehydrogenation of the nanoconfined LiBH$_4$ in PMMA–co–BM–MWCNT composite.
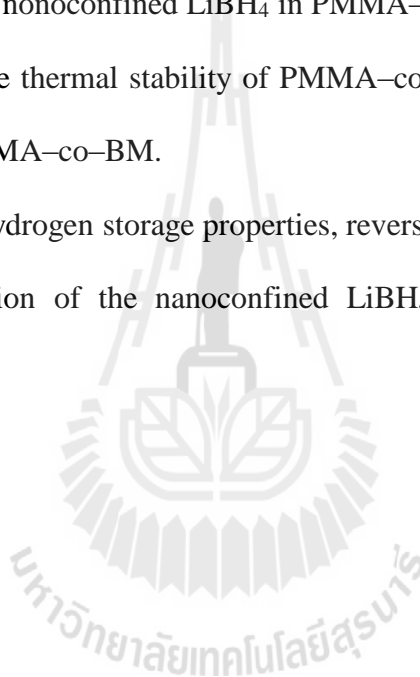
CHARPTER III

EXPERIMENTS

3.1 Sample preparation

3.1.1 Purification of tetrahydrofuran (THF)

Tetrahydrofuran (THF) (HPLC grade, QRëC^{TM}) was pre–dried overnight by molecular sieves. Sodium metal (Na) and benzophenone of 5.0017 and 20.0006 g, respectively, were added to 500.0 mL of pre–dried THF (Schwartz, 1978). The mixture was refluxed under nitrogen atmosphere at 80 °C until a deep blue color was obtained. The mixture was distilled at 70 °C under nitrogen atmosphere to obtain anhydrous THF.

3.1.2 Precipitation of poly (methyl methacrylate)−co−butyl methacrylate

Poly (methyl methacrylate)–co–butyl methacrylate (PMMA–co–BM) (Mw = 75,000 g/mol, Sigma Aldrich), shortly named PcB in this work of 20.4890 g was dissolved in 100.0 mL anhydrous THF with continuous stirring to obtain homogeneous polymer solution (20.0 % w/v). The PcB solution was precipitated in distillated n–hexane (AR grade, QRëC^{TM}) and dried at 90 °C for 24 h in vacuum oven to obtained dried PcB polymer powder.

3.1.3 Synthesis of nanoconfined LiBH$_4$ in PcB

The PcB polymer solution was prepared by dissolving 5.0656 g of PcB powder in 20.00 mL anhydrous THF with continuous stirring. Lithium borohydride (LiBH$_4$) solution (2 M in THF, Sigma Aldrich) of 15.00 mL was added to PcB polymer solution. The mixture was stirred for approximately 10 min at room temperature in the glove box to

obtain transparent gel. The gel was dried at room temperature in the glove box for several

days to achieve nanoconfined sample of $LiBH_4$ in PcB, denoted as nano $LiBH_4$–PcB.

3.1.4 Synthesis of nanoconfined LiBH₄ in PcB-MWCNT composite

PcB polymer powder of 5.0745 g was dissolved in 20.00 mL anhydrous THF and

stirred to obtain PMMA−co−BM polymer solution. Multi–walled carbon nanotube

(MWCNT) of 0.0055 g (0.10 wt. % of MWCNT with respect to PcB content) was dispersed

homogeneously in PcB polymer solution by using ultra sonication for several hours. The

clear solution of PcB containing MWCNT was added with 10.00 mL $LiBH_4$ solution (2 M

in THF, Sigma Aldrich) in the glove box and continuously stirred for approximately 10

min to obtain transparent gel. The gel was dried at room temperature in the glove box to

obtain nanoconfined $LiBH_4$ in PcB composite, denoted as nano $LiBH_4$–PcB–MWCNT.

3.2 Characterization

3.2.1 Scanning electron microscopy (SEM) and energy−dispersive X−ray spectroscopy (EDS)

Scanning electron microscopy (SEM) was carried out with an Auriga (Zeiss,

Germany) at Institute of Materials Research, Helmholtz−Zentrum Geesthacht, Germany.

Nanoconfined sample of $LiBH_4$–PcB–MWCNT was deposited on the sample holder by

using silver glue (in *n*-butyl acetate). The powder sample was coated with platinum (Pt)

by using sputtering technique with a current of 30 mA for 30 s under vacuum. An

energy−dispersive X−ray spectroscopy (EDS)–elemental mapping were managed by an

apparatus from EDAX Inc., USA. Smart SEM and EDS Genesis programs were used for

morphological studies and elemental analysis of the sample, respectively.

3.2.2 Differential scanning calorimetry (DSC) and mass spectroscopy (MS)

Dehydrogenation behaviors of nano $LiBH_4$-PcB-MWCNT was measured by simultaneous thermal analysis (STA) (a Netzsch, STA 449 F3 Jupiter). The signal of hydrogen release during dehydrogenation was simultaneously detected by mass spectrometer (a QMS 403C Aëolos Mass spectrometer, NETZSCH). The sample weight of about 5–10 mg was loaded into Al_2O_3 crucible in the glove box under argon atmosphere. The crucible was placed in a glass bottle and sealed by parafilm to protect oxidation during transportation from the glove box to the apparatus. The samples were heated from 30 to 300 °C ($\Delta T/\Delta t = 5$ °C/ min) with nitrogen purge rate of 50 mL/min.

3.2.3 Kinetic measurement

De/rehydrogenation kinetics and hydrogen reproducibility of nanoconfined samples were studied by using a laboratory scale setup of a Sievert–type apparatus (Figure 3.1). The powder sample of ~50–100 mg was packed in a high pressure stainless steel sample holder (316SS, Swagelok) under argon atmosphere in the glove box, and transferred to the Sievert–type apparatus. Two K–type thermocouples (-250−1,300 °C, SL heater) were attached to the sample holder and to the furnace for measuring the temperature change of the system during de/rehydrogenation. Pressure transducers (C206, Cole Parmer) in the pressure range of 0–500 psig and 0–3000 psig were used to measure the pressure changes due to hydrogen desorption and absorption, respectively. Thermocouples and pressure transducers were connected to an AI210I module convertor data logger (from Wisco), measuring and transferring (every 1 s) the pressure and temperature changes of the sample to the computer for further evaluation. Dehydrogenation of the samples was done under an isothermal condition of 120 °C (vacuum) via a furnace controlled by a PID

temperature controller. In the case of rehydrogenation, the dehydrogenated powder sample

was pressurized under 60 bar H_2 (purity= 99.999%) at 120 °C for 12 h. The amount of

hydrogen release and uptake is calculated based on the amount of $LiBH_4$ in the sample by

using ideal gas law (see in appendix A).
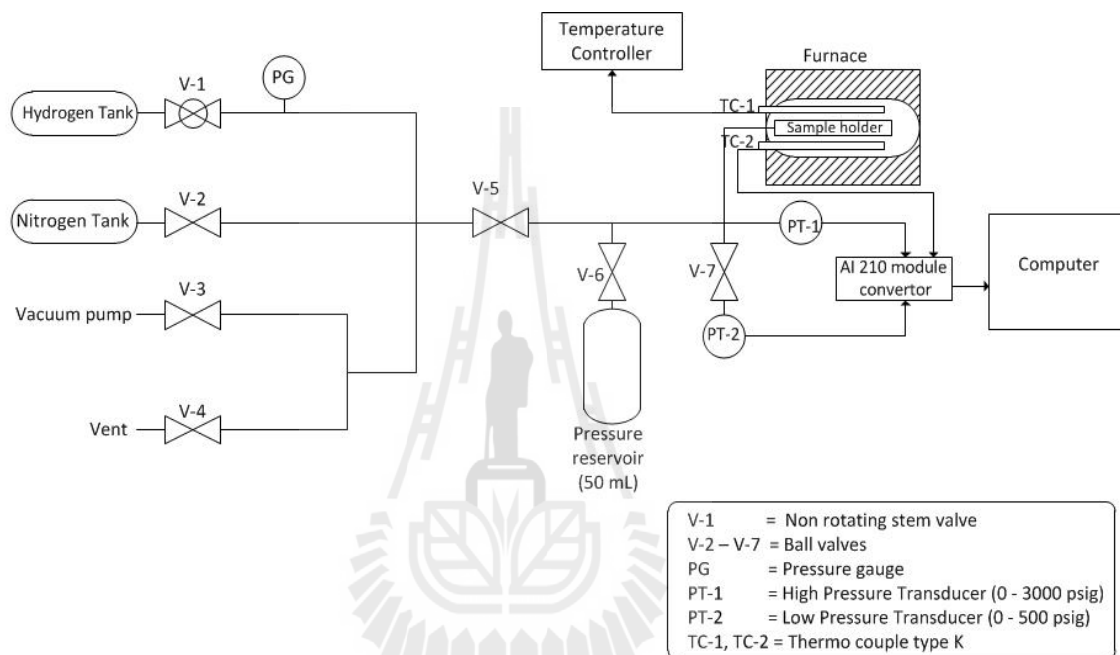
Figure 3.1 Schematic diagram of Sieverts–type apparatus used in this research project
(Gosalawit-Utke et al., 2014).

3.2.4 Gas analysis

The analyses of gases released during dehydrogenation of nano $LiBH_4$–PcB and

nano $LiBH_4$–PcB–MWCNT were carried out at Pavia Hydrogen Lab., C. S. G.I.,

Department of Chemistry, Physical Chemistry Division, University of Pavia, Italy. The

experiment was performed by connecting a manometric PCTPro–2000 apparatus with a

residual gas analyzer (RGA200, Setaram, France). The powder sample (~200 mg) was

loaded in the sample holder and transferred to the PCTPro–2000 apparatus. The

measurement was done by heating the powder sample from room temperature to 300 °C (5 °C/min) under vacuum.

3.2.5 Fourier transform infrared spectroscopy (FT-IR)

Fourier transform infrared spectroscopy (FTIR) of standard samples (pristine $LiBH_4$, PMMA−co−BM and PMMA−co−BM−MWCNT composite) and nanoconfined $LiBH_4$−PcB−MWCNT and $LiBH_4$−PcB at different stages of before and after dehydrogenation and after rehydrogenation were performed by using a Bruker, Model Tensor 27. The sample was ground with anhydrous KBr (1:10 weight ratio of sample: anhydrous KBr) and pressed under 3 tons for 2 min to obtain KBr pellet. FTIR spectrum of each sample was obtained by assembling KBr pellet containing the sample in the FTIR machine on the direction of infrared. The spectrum was recorded in the range of 4000–400 cm^{-1} with 32 scans at room temperature.

3.2.6 X-ray photoelectron spectroscopy (XPS)

X-ray photoelectron spectroscopy (XPS) was carried out at the Siam Photon Laboratory, BL3.2a in the Synchrotron Light Research Institute (Public Organization), Nakhon Ratchasima, Thailand. The powder sample of pristine $LiBH_4$, nano $LiBH_4$−PcB and nano $LiBH_4$−PcB−MWCNT were held on the sample holders by using carbon glue tape. Prior to the measurements, all prepared samples were placed in an ultrahigh vacuum chamber for approximately 6 h. The photon energy of 400 eV was used to detect the signals of Li $1s$ and B $1s$. Each element was investigated at the kinetic energy step of 0.1 eV for 5 scans by using a CLAM2 analyzer. The multi spectra were analyzed by using a macro XPS MS Excel 2007 (Windows XP) software.

CHAPTER IV

RESULTS AND DISCUSSION

4.1 Nanoconfinement of LiBH$_4$ in PcB composite

To study sample morphology as well as elemental distribution and analysis, SEM and EDS techniques were performed. Figure 4.1 (A) shows sample morphology where elemental was taken into account. The homogeneous dispersion of boron atoms (from LiBH$_4$) in nanoscale is observed on the surface of the sample, confirming the existence of LiBH$_4$ in PcB−MWCNT composite matrix (Figure 4.1 (B)). Figure 4.1 (C) reveals the distribution of carbon atoms from PcB −MWCNT composite, where the agglomeration of MWCNT is represented by green-bright area. Figure 4.1 (D) exhibits the amount of carbon (C) and oxygen (O), which are the main elements in PcB −MWCNT structure, together with boron (B) of LiBH$_4$. However, signal of lithium (Li) of LiBH$_4$ is not detected due to the limitation of EDS technique to light element.
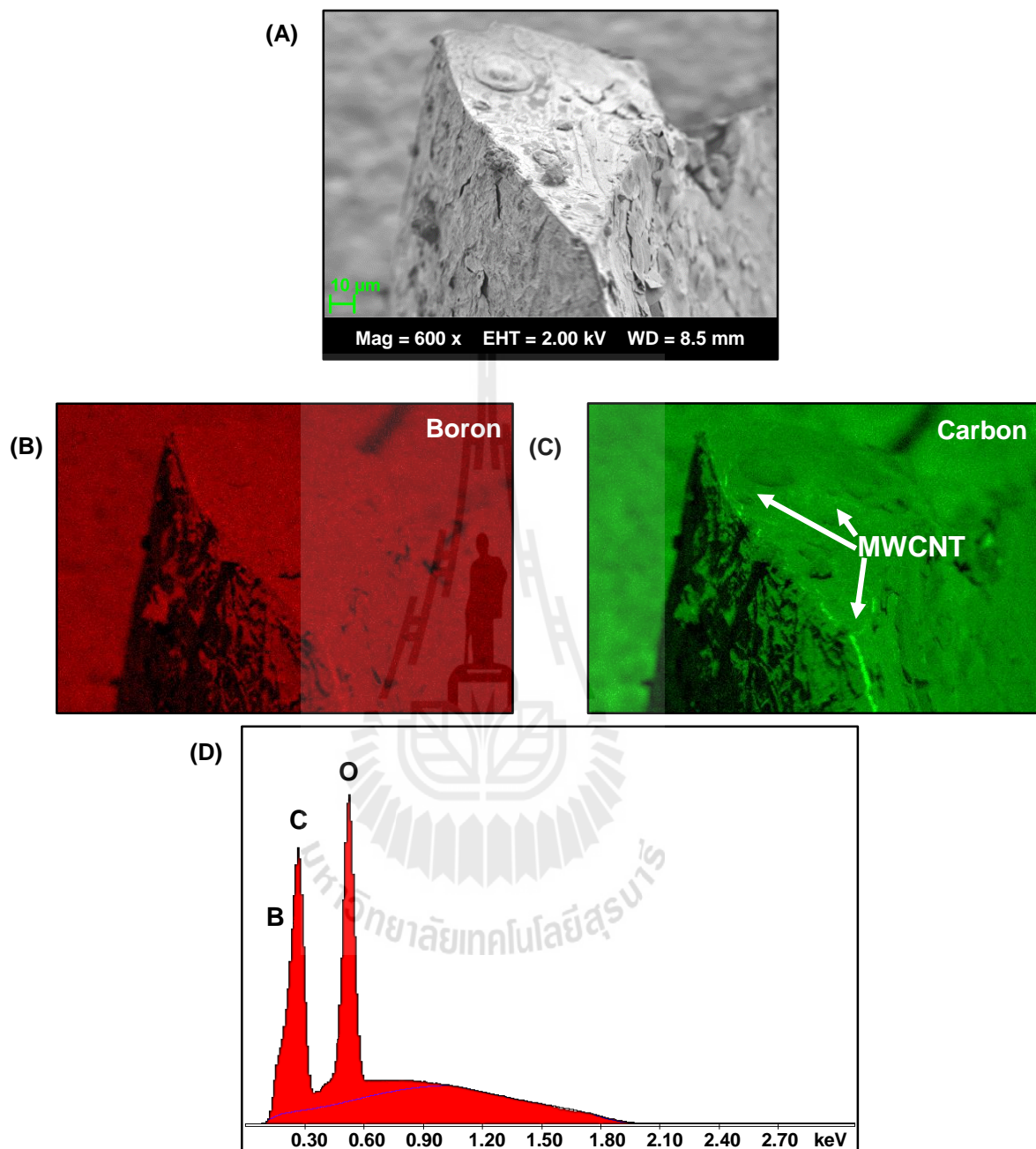
Figure 4.1 SEM image of nano LiBH$_4$-PcB-MWCNT composite (A), Boron mapping (B), Carbon mapping (C), and quantitative elemental analysis (D).

4.2 Dehydrogenation and reversibility

To investigate the hydrogen desorption behavior of nanoconfined sample, DSC measurements and H_2 mass spectroscopy were performed. From DSC results (Figure 4.2), nano LiBH$_4$−PcB−MWCNT exhibits an exothermic peak at 138 °C together with H_2 MS signal, corresponded to the combination of dehydrogenation and interaction between polymer matrix and LiBH$_4$ as similar as nanoconfined sample of LiBH$_4$−PcB (without MWCNT) previously reported (Gosalawit−Utke et al., 2014).
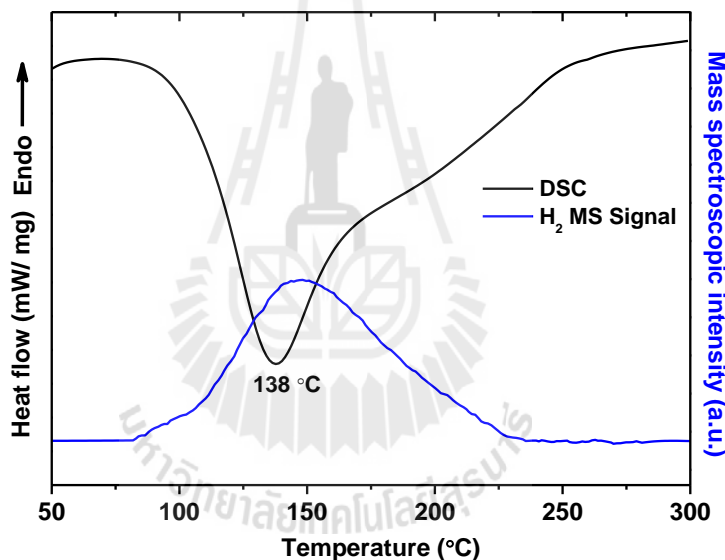
Figure 4.2 Dehydrogenation profile and H_2 Mass of nano LiBH$_4$–PcB–MWCNT composite

The theoretical hydrogen storage capacity of nanoconfined samples calculated from the amount of all components in the samples are shown in Table 4.1. Nano LiBH$_4$–PcB containing 11.5 wt. % of LiBH$_4$ gives 1.60 wt. % H_2 as theoretical hydrogen storage capacity, while that of nano LiBH$_4$–PcB–MWCNT consisting of 0.1 wt. % of MWCNT and 8.0 wt. % of LiBH$_4$, is 1.1 wt. % H_2 (Table 4.1).

Table 4.1 Amount of components and theoretical hydrogen storage capacity of nanoconfined samples

Nanoconfined samples	Amount of components			Theoretical H$_2$ storage capacity (wt. %)
	PcB (g)	MWCNT (wt. %)	LiBH$_4$ (wt. %)	
nano LiBH$_4$-PcB	5.0656	-	11.5	1.60
nano LiBH$_4$-PcB-MWCNT	5.0745	0.1	8.0	1.10

To study dehydrogenation kinetics, reversibility, and hydrogen reproducibility, titration measurements of nanoconfined samples were performed by Sievert–type apparatus. Dehydrogenation and rehydrogenation were carried out at the same temperature of 120 °C under vacuum and 60 bar H$_2$, respectively. Regarding the hydrogen contents desorbed during cycling, the results of nano LiBH$_4$–PcB are normalized by thermal degradation of PcB (at 120 °C under vacuum for 6 h), while those of nano LiBH$_4$–PcB–MWCNT are by degradation of PcB–MWCNT composite under the same temperature, pressure, and time condition. From Figure 4.3, nano LiBH$_4$–PcB released 0.78 wt. % H$_2$ (48.8% of theoretical hydrogen storage capacity) during the 1st dehydrogenation within 3 h. The inferior hydrogen storage capacity to the theoretical value (1.60 wt. % H$_2$) can be due to the interaction between LiBH$_4$ and methoxy (–OCH$_3$) branches of PcB formed during sample preparation, discussed and reported in the previous studies (Gosalawit−Utke et al., 2014). For the 2nd cycle, it provides only 0.32 wt. % H$_2$ (20% of theoretical hydrogen storage capacity). Significant reduction in hydrogen content released in the 2nd dehydrogenation with respect to the 1st one can be due to (i) greater interaction between LiBH$_4$ and PcB matrix after cycling as previously reported (Gosalawit−Utke et al., 2014)

and (ii) thermal degradation of PcB polymer matrix during cycling under temperature and pressure.
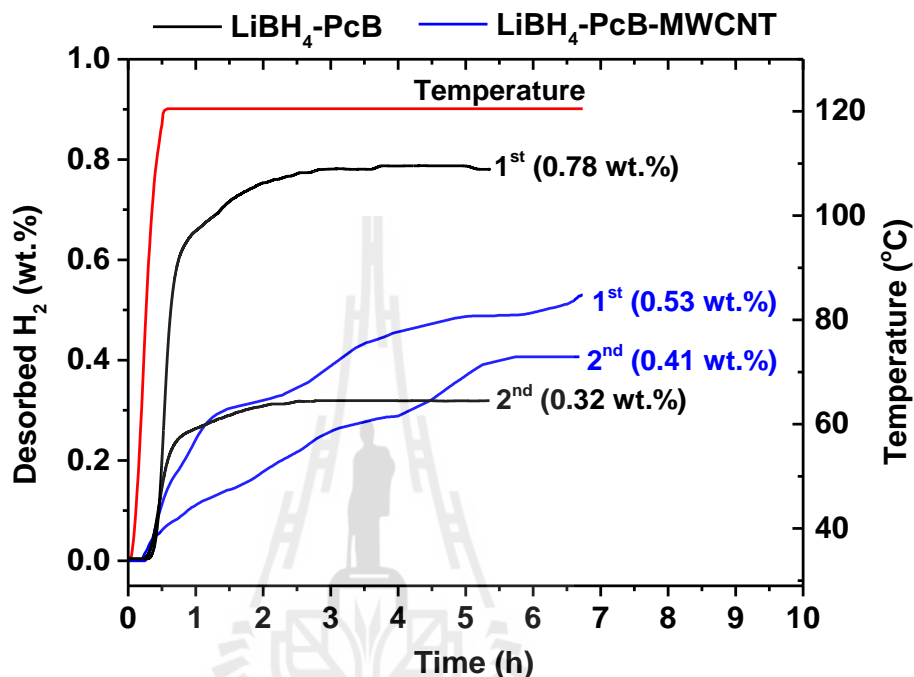
Figure 4.3 Dehydrogenation kinetics of nanoconfined samples at 120 °C, under vacuum.

Nano LiBH$_4$–PcB–MWCNT releases 0.53 and 0.41 wt. % H$_2$; i.e., approximately 48.4 and 37.3% of theoretical hydrogen storage capacity (1.10 wt. % H$_2$), after 6 h during the 1st and 2nd cycles, respectively. The deficient hydrogen storage capacity as compared with theoretical value can be due to the interaction between LiBH$_4$ and PcB as in case of nano LiBH$_4$–PcB. It should be noted that the 2nd dehydrogenation of nano LiBH$_4$–PcB–MWCNT can considerably preserve hydrogen content reproducibility (37.3%) as compared with that of nano LiBH$_4$–PcB (20%). This can be due to thermal stability improvement of nano LiBH$_4$–PcB after compositing with MWCNT, further confirmed in gas analyses. However, the slow kinetics observed in nano LiBH$_4$–PcB–MWCNT could

be due to the random arrangement of MWCNT in PcB hindering the diffusion of H_2 in the polymer matrix.

4.3 Thermal stability

To study thermal stability of PcB matrix of nanoconfined samples with and without MWCNT doping during dehydrogenation, gas analyses were performed.
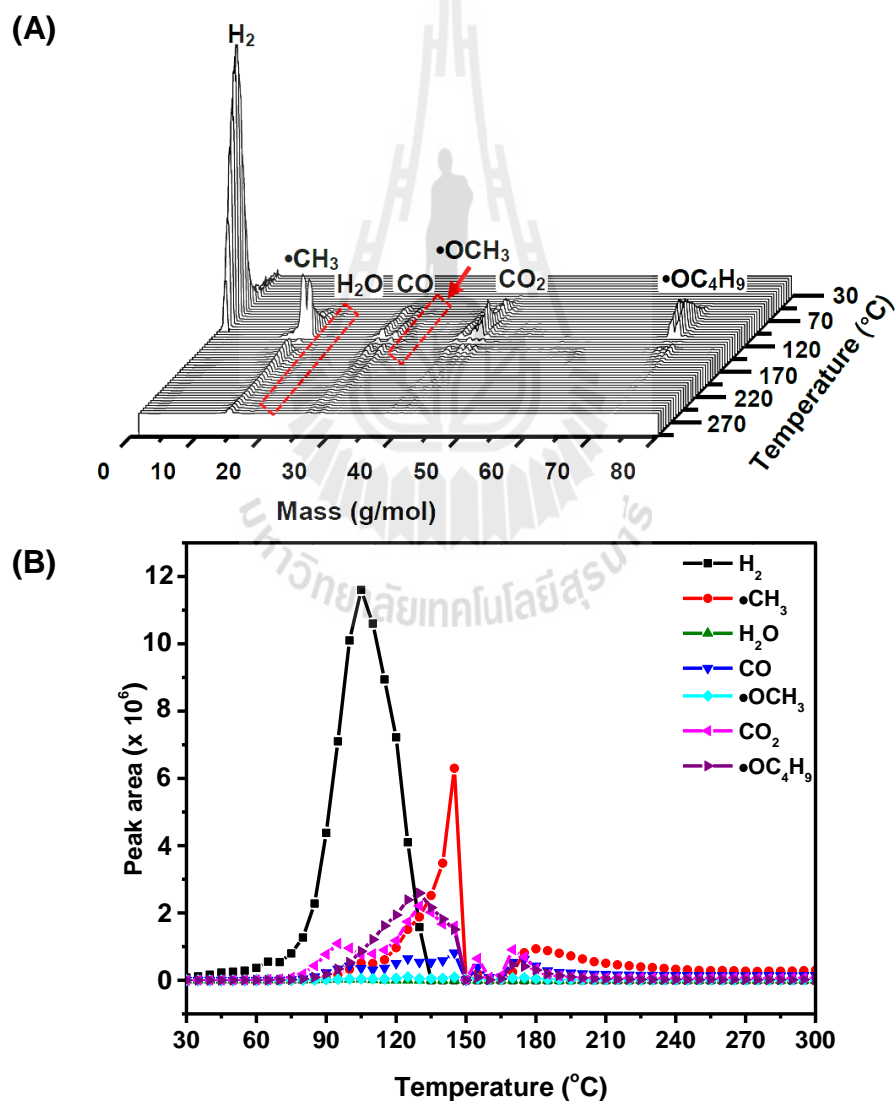
Figure 4.4 Gas analysis during dehydrogenation of nano $LiBH_4$–PcB (A) and plot between peak areas of gas desorption of nano $LiBH_4$–PcB and temperature (B).

From Figure 4.4, nano LiBH$_4$−PcB release hydrogen (H$_2$) as the main gas in the temperature range of 30−300 °C together with carbon monoxide (CO), carbon dioxide (CO$_2$), methyl radical (CH$_3$•), metoxy radical (CH$_3$O•), and butoxy radical (CH$_3$CH$_2$CH$_2$CH$_2$O•). It was reported that CO, CO$_2$, CH$_3$•, and CH$_3$O• are products of thermal degradation of PMMA (Kashiwaki et al., 1986; Kashiwaki et al., 1989). In our casse, butoxy radical is also detected due to thermal degradation of buthoxy branches in PcB. Therefore, this can be concluded that not only dehydrogenation occurs in the temperature range of 30−300 °C, but also partial thermal degradation of PcB.

Figure 4.4(B) shows onset dehydrogenation temperature of nano LiBH$_4$–PcB at 80 °C together with the other gases and reaches its peak at 105 °C. The H$_2$ signal of nano LiBH$_4$–PcB ended at 135 °C, while the gases from thermal decomposition of polymer matrix are still continued. It was reported in the previous work that the partial degradation of PcB polymer matrix probably caused to the reduction in hydrogen reproducibility of nanoconfined samples (Gosalawit et al., 2014).

In the case of nano LiBH$_4$−PcB−MWCNT (Figure 4.5), it reveals the peaks of gases desorption from both dehydrogenation and thermal decomposition of PcB as obtained in nano LiBH$_4$–PcB (Figure 4.4 (A)). From Figure 4.5 (B), it is found that the hydrogen starts to release at 85 °C. The peak temperature is at 130 °C and it ends at ~200 °C. The peak area of gases released from partial degradation of PcB starts to increase at ~120 °C, approximately 40 °C higher than that of nano LiBH$_4$–PcB. This suggests that the thermal stability of PcB polymer matrix is improved by compositing with 0.1 wt. % of MWCNT.
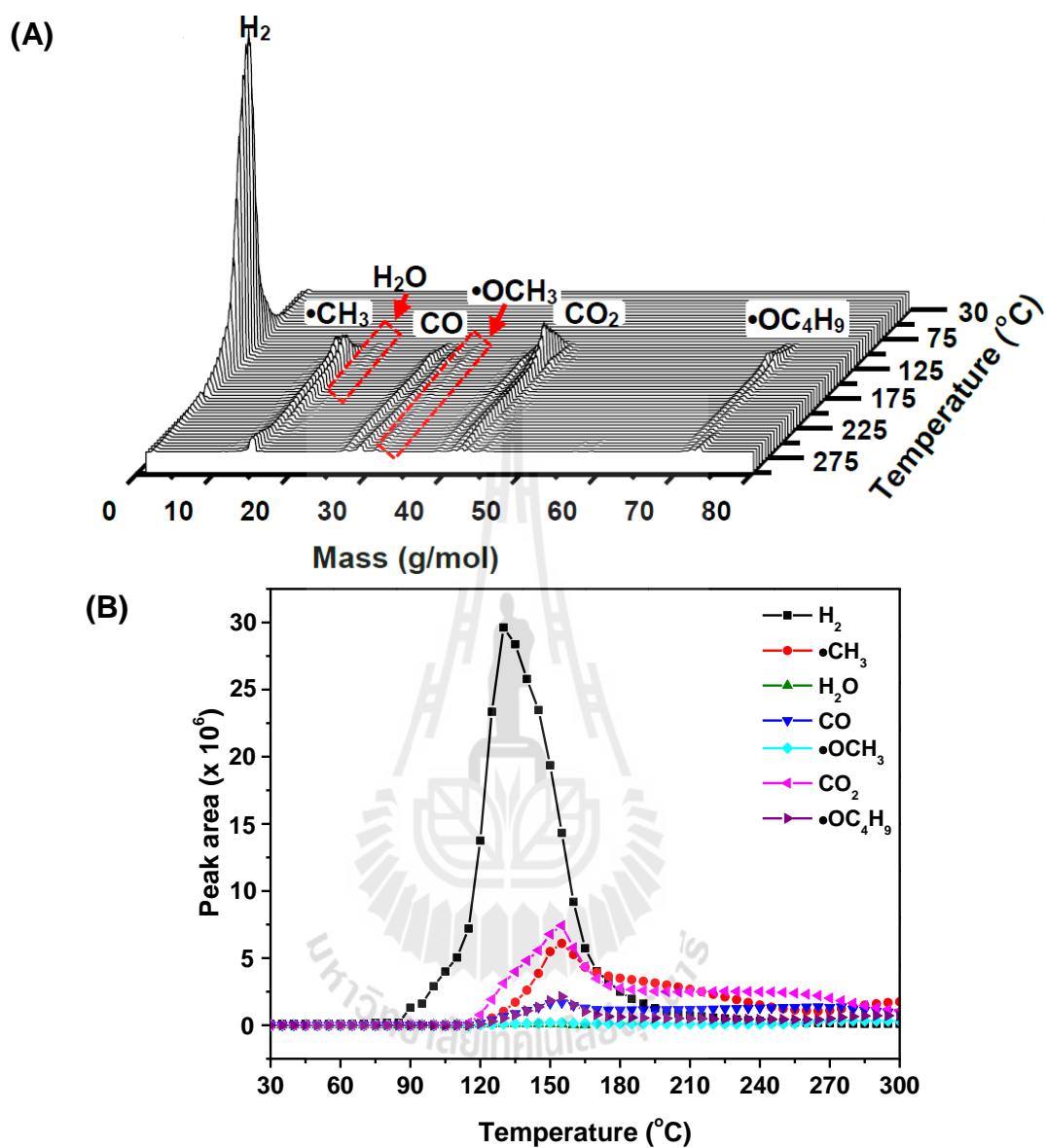
Figure 4.5 Gas analysis during dehydrogenation of nano LiBH₄–PcB–MWCNT (A) and

plot between peak areas of gas desorption of nano LiBH₄–PcB–MWCNT and temperature

(B).

From the gas analysis results (Figures 4.4 and 4.5), the dehydrogenation temperature and amounts of gases desorbed due to thermal degradation of PcB at 120 °C are summarized in Table 4.2. With respect to the peak area of H_2 at 120 °C, relative amount of $CH_3\bullet$, CO, CO_2, $CH_3O\bullet$, and $CH_3CH_2CH_2CH_2O\bullet$ with respect to H_2 of nano $LiBH_4$–PcB are 13.4, 6.9, 0.8, 16.3, and 26.9 %, respectively, while those of nano $LiBH_4$–PcB–MWCNT are 0.9, 1.1, 0.2, 5.6, and 0.7%, respectively. The relative amount of gases release from degradation of PcB is totally 64.3 and 9.0% for nano $LiBH_4$–PcB and nano $LiBH_4$–PcB–MWCNT, respectively. From Table 4.2, it can be concluded that the thermal stability of nano $LiBH_4$–PcB is increased by compositing with MWCNT.

Table 4.2 Dehydrogenation temperature of nanoconfined samples and amount of gas desorption from thermal degradation of PcB with respect to H_2 content at 120 °C.

Nanoconfined samples	Dehydrogenation temperature (°C)			Gas desorption from thermal degradation of PcB with respect to H_2 at 120 °C (%)						
	T_i	T_p	T_f	$\bullet CH_3$	H_2O	CO	$\bullet OCH_3$	CO_2	$\bullet OC_4H_9$	Total
nano $LiBH_4$–PcB	80	105	135	13.4	0	6.9	0.8	16.3	26.9	64.3
nano $LiBH_4$–PcB–MWCNT	85	130	190	0.9	0.5	1.1	0.2	5.6	0.7	9.0

T_i = Onset temperature, T_p = peak temperature, and T_f = end temperature

4.4 Reaction mechanisms and reversibility

In order to confirm that LiBH$_4$ was confined in PcB−MWCNT composite and PcB polymer matrix and to understand the reaction mechanisms during de/rehydrogenation, nano LiBH$_4$−PcB and nano LiBH$_4$−PcB−MWCNT together with standard materials related to nanoconfined samples were preliminary characterized by FT−IR technique.
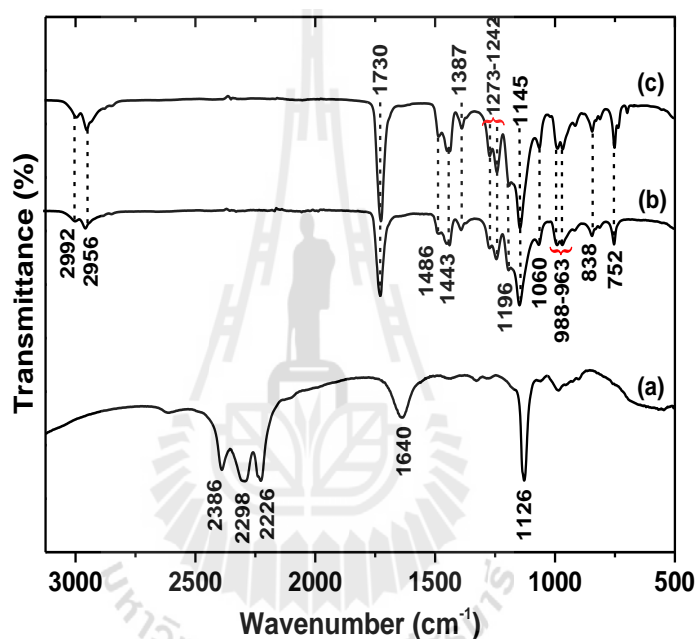
Figure 4.6 FT−IR spectra of LiBH$_4$ (a), PcB (b), and PcB−MWCNT (c).

For bulk LiBH$_4$, Figure 4.6 (a) reveals the triplet peaks of B−H bond stretching and bending at 2395–2234 and 1125 cm^{-1}, respectively. The peak at 1640 cm^{-1} refers to O−H bond from the contamination of moisture in air during the experiments. PcB (Figure 4.6 (b)) and PcB−MWCNT (Figure 4.6 (c)) show vibrational peaks corresponding to C−H stretching at 2956–2992 cm^{-1} and C=O stretching of ester group at 1730 cm^{-1}. The absorption peaks around 1448 and 1486 cm^{-1} belong to asymmetric bending vibrations of C−CH$_3$ and C−CH$_2$ bonds, respectively (Namouchi et al., 2009). The vibrational peaks at

1387 and 752 cm^{-1} can be attributed to the α–CH$_3$ group vibrations. The two doublet bands at 1273–1242 and 1196–1154 cm^{-1} are C–O stretching vibrations of ester group. The vibrational peaks at 1060, 988–963 and 838 cm^{-1} are the characteristic peaks of methylene wagging, main chain C–C stretching and C=O deformation, respectively (Velasco–Santos et al., 2003; Matsushita et al., 2000). Due to similar FT–IR spectra of both PcB and PcB–MWCNT composite, no chemical interaction between PcB and MWCNT is observed. This results in agreement with previous report (Bal et al., 2007; Swain et al., 2010). The interaction of polymer matrix and MWCNT is only weak van der waals bonding between interface of nanotubes and the PcB matrix. Thus, the addition of MWCNT could increase the thermal decomposition temperature of the polymer matrix due to their constraint effect on the polymer segments and chains (Swain et al., 2010).

After nanoconfinement, nano LiBH$_4$–PcB exhibits all characteristic peaks of both LiBH$_4$ and PcB polymer matrix, confirming the existance of LiBH$_4$ in PcB polymer matrix (Figure 4.7 (A)). The sharp peak of B–O bond at 1370 cm^{-1} and a shoulder at 1707 cm^{-1}, in agreement with the B---OCH$_3$ interaction formed between [BH$_4$]$^-$ and PcB and Li$^+$---O=C interaction respectively, are observed as discussed in the previous report (Gosalawit–Utke et al., 2014). The interactions between LiBH$_4$ and PcB polymer matrix refer to partial dehydrogenation of LiBH$_4$ during nanoconfinement, leading to reduction of hydrogen storage capacity in 1st dehydrogenation cycle.

After dehydrogenation at 120 °C under vacuum, the signals of B–H vibrations disappear, hinting at complete dehydrogenation of nano LiBH$_4$–PcB. For the spectrum after rehydrogenation at 120 °C under 60 bar H$_2$, slight signals of LiBH$_4$ are observed, referring to partial reversibility of this sample. In the case of nano LiBH$_4$–PcB–MWCNT, vibrational peaks of B-H stretching (2386, 2293, and 2226 cm^{-1}) and bending (1126 cm^{-1})

of LiBH$_4$ are significantly detected together with those of PcB in the sample before desorption (Figure 4.7 (B)). A small shoulder at 1708 cm^{-1} observed in nano LiBH$_4$–PcB–MWCNT refer to the interaction of carbonyl group of PcB with Li$^+$ ion of LiBH$_4$ as in case of nano LiBH$_4$–PcB. Regarding the sample before desorption of nano LiBH$_4$–PcB (Figure 4.7 (A)), vibrational peak of B–O bonds from B---OCH$_3$ interaction is confirmed by the sharp peak at 1383 cm^{-1}.
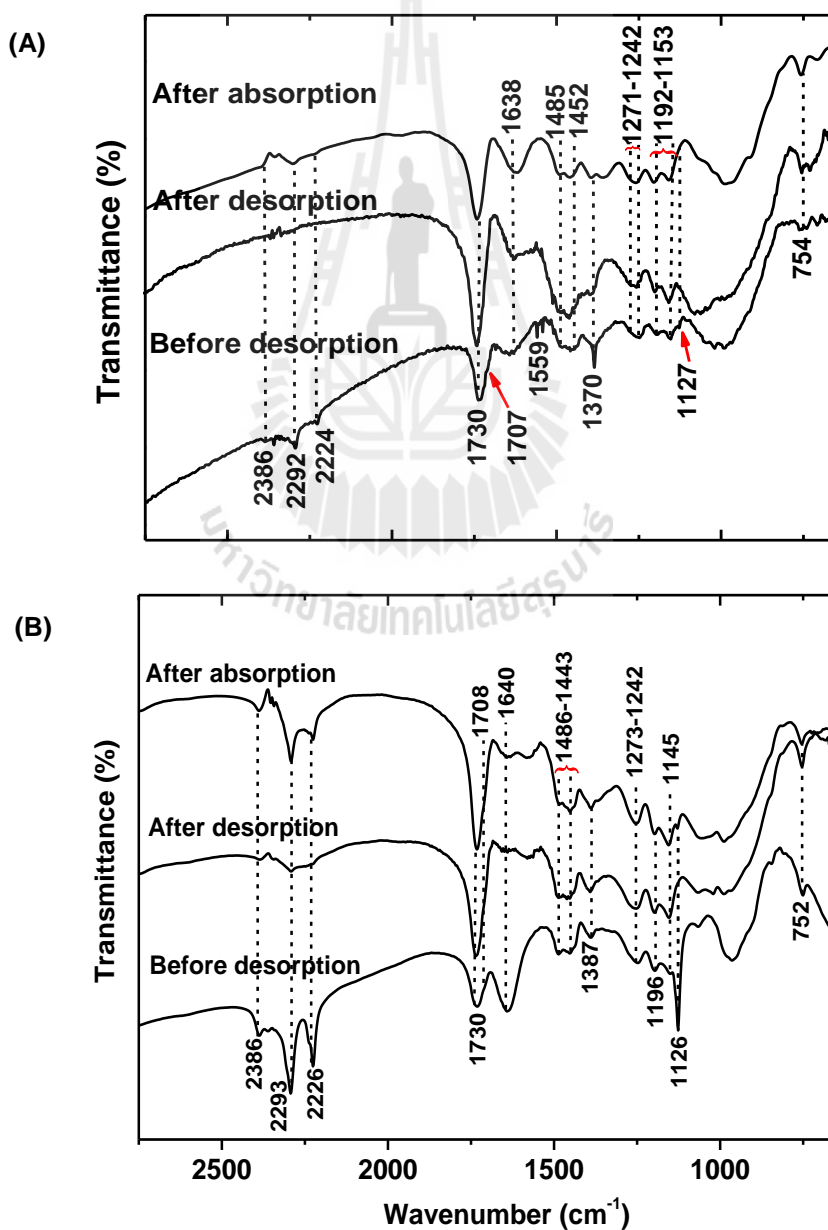
Figure 4.7 FT–IR spectra of nano LiBH$_4$–PcB (A) and nano LiBH$_4$–PcB–MWCNT (B).

However, there is only a small peak at 1387 cm^{-1} in the case of nano LiBH$_4$–PcB–MWCNT. Together with a peak at 752 cm^{-1}, the small peak at 1387 cm^{-1} of nano LiBH$_4$–PcB–MWCNT attributes mainly to characteristic vibrational peak of α–methyl group in PcB (Figure 4.6 (b)). Due to insignificant signal of B---OCH$_3$ interaction and considerably vibrational peak of B–H bonds of nano LiBH$_4$–PcB–MWCNT, it should be noted that the interaction between [BH$_4$]$^-$ and –OCH$_3$ (B---OCH$_3$) can be reduced by adding small amount of MWCNT.   After dehydrogenation at 120 °C under vacuum, the peak intensity of B–H vibrations of LiBH$_4$ decrease and the peak intensity is recovered after rehydrogenation at 120 °C under 60 bar H$_2$. The reproducibility of LiBH$_4$ clearly confirms that reversibility of nano LiBH$_4$–PcB–MWCNT.

4.5 LiBH$_4$/ PcB interaction

Nanoconfined LiBH$_4$ in PcB–MWCNT composite is hypothesized not only to improve thermal stability of polymer host, but also to reduce the interaction between LiBH$_4$ and PcB. As discussed in the previous work (Gosalawit–Utke et al., 2014), Figure 4.8 reveals the interaction between LiBH$_4$ and PcB polymer branched chains at –OCH$_3$ and C=O positions, i.e., H$_{(4-x)}$B---(OCH$_3$)$_x$, B---(OCH$_3$)$_4$, and Li$^+$---O=C. The formations of H$_{(4-x)}$B---(OCH$_3$)$_x$ and B---(OCH$_3$)$_4$ interactions result in the cross linking of PcB polymer, observed as gel formation during sample preparation. The formation of LiBH$_4$/PcB interaction leads to partial dehydrogenation of LiBH$_4$ during sample preparation, resulting in the reduction of hydrogen storage capacity of both nanoconfined samples in 1st dehydrogenation cycle.
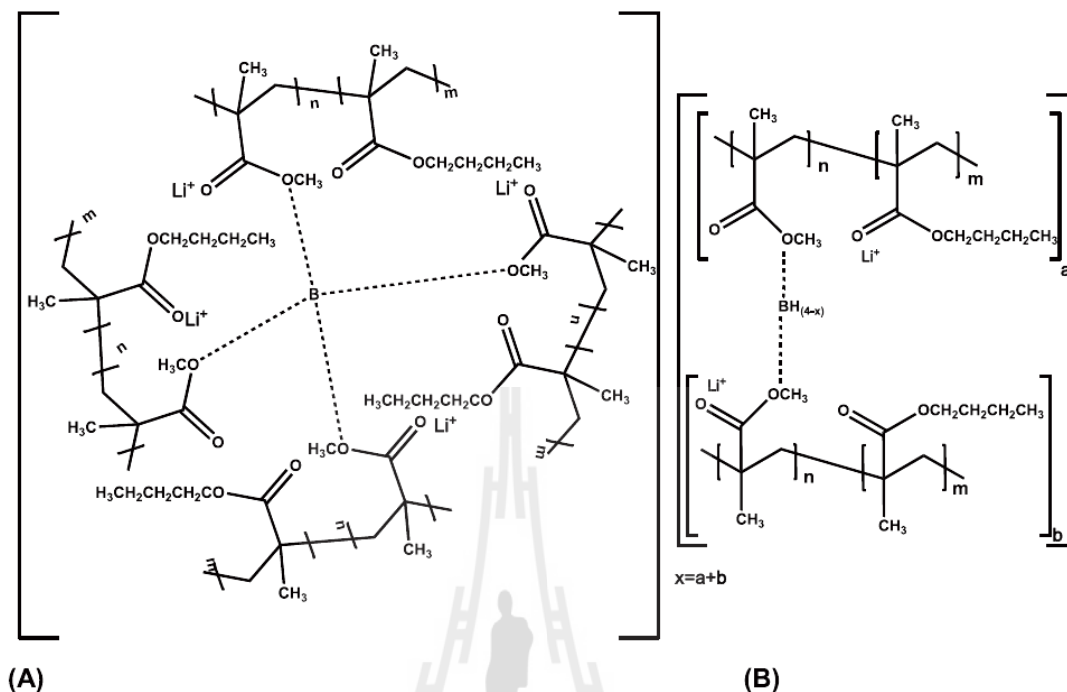
Figure 4.8 Interactions between LiBH$_4$ and PcB polymer chains at −OCH$_3$ position (H$_{(4-x)}$B---(OCH$_3$)$_x$ and B---(OCH$_3$)$_4$, where (a + b= x) and at C=O (Li+---O=C) (Gosalawit–Utke et al., 2014).

To confirm that the LiBH$_4$/PcB interaction was reduced after MWCNT doping, the curve fitting and peak area of vibrational peaks belonging to B–H stretching (LiBH$_4$) and C=O stretching (PcB) were calculated from FT–IR spectra of nanoconfined samples (Figure 4.9 and Table 4.3). From Table 4.3, the υ(B–H)/υ(C=O) of nano LiBH$_4$–PcB is 0.6, while that of nano LiBH$_4$–PcB–MWCNT is 2.7. This result indicated that the partial dehydrogenation of nano LiBH$_4$–PcB during nanoconfinement is reduced by MWCNT doping.
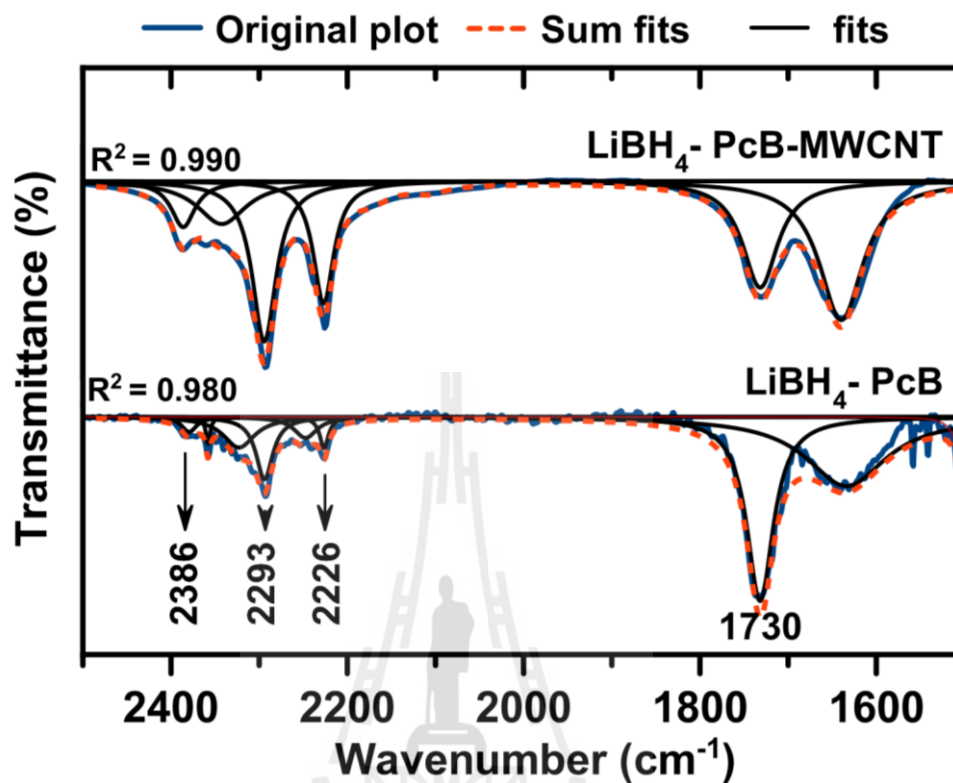
Figure 4.9 FT−IR curve fitting of B−H and C=O stretching peaks of nanoconfined samples before H$_2$ desorption.

Table 4.3 Peak area of B−H and C=O stretching peaks of nanoconfined samples, calculated from curve fitting technique.

Samples	Peak area		υB-H/ υC=O ratio
	υ(B-H) (2226-2386 cm^{-1})	υ(C=O) (1730 cm^{-1})	
Before desorption			
nano LiBH$_4$−PcB	109.5	171.2	0.6
nano LiBH$_4$−PcB−MWCNT	12.2	4.5	2.7

X-ray photoelectron spectroscopy (XPS) was used to confirm the ability of PcB and PcB–MWCNT to prevent deterioration of $LiBH_4$ by oxidation in air and humidity. In addition, XPS technique is an alternative way to prove the reduction of $LiBH_4$/PcB interaction in this study. In Figure 4.10 (a), Li 1s spectra of pristine $LiBH_4$ exhibits the signal of Li_2O at 55 eV (Deprez et al., 2011). In the case of B 1s, the signal of B_xO_y (x/y = 3) and B_2O_3 are observed at 187 eV and 192 eV, respectively (Figure 4.10 (a) (Deprez et al., 2011). The formation of Li_2O, B_xO_y (x/y = 3), and B_2O_3 is due to the reaction of $LiBH_4$ and O_2 and/or humidity in air. In the case of nano $LiBH_4$–PcB and nano $LiBH_4$– PcB–MWCNT (Figures 4.10 (b) and (c)), the Li 1s signal of LiH and $LiBH_4$ are observed at 54 and 56 eV, respectively (Haipinga et al., 2011; Fang, et al., 2011).
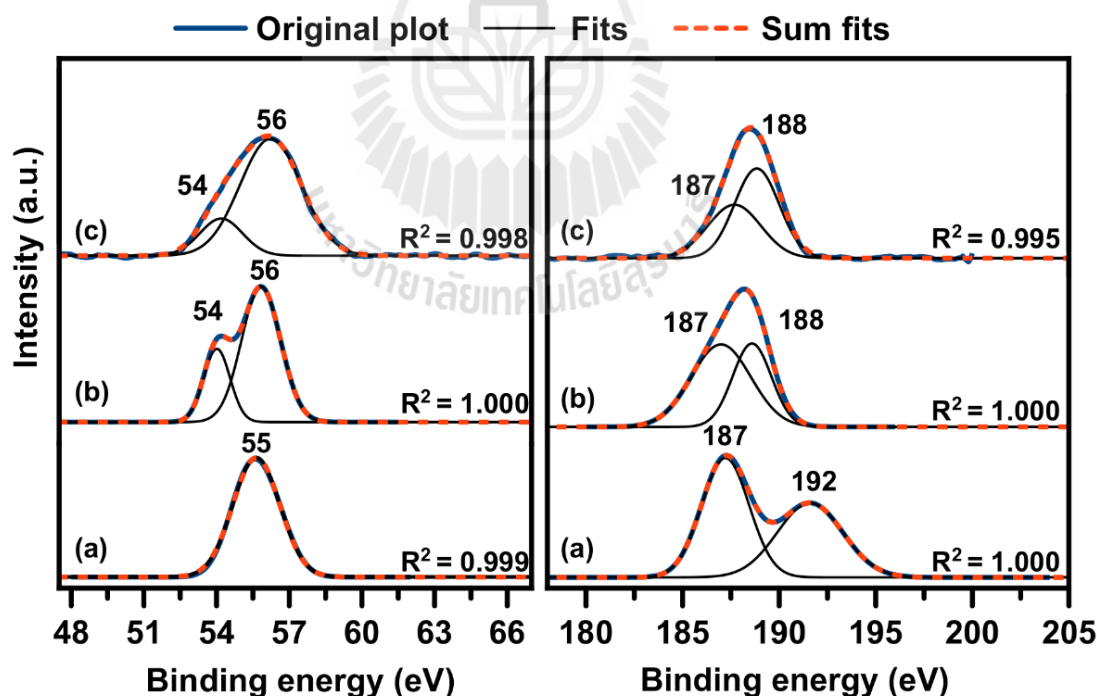
Figure 4.10 Li 1s and B 1s XPS spectra of pristine $LiBH_4$ (a), nano $LiBH_4$–PcB (b), and nano $LiBH_4$–PcB–MWCNT (c).

For B 1s spectra, the characteristic peaks of B_xO_y (x/y = 3) and $LiBH_4$ are observed at 187 and 188 eV, respectively (Haipinga et al., 2011; Deprez et al., 2011). Therefore, the signal of $LiBH_4$, observed in Li 1s and B 1s spectra of nano $LiBH_4$–PcB and nano $LiBH_4$–PcB–MWCNT, confirms the stability in air of $LiBH_4$ after nanoconfinement in polymer matrix.

With respect to the signal of B_xO_y (x/y = 3) in B 1s spectrum, it should be refered to the interactions between B atoms (from $[BH_4]^-$) of $LiBH_4$ with methoxy groups and/or buthoxy group of PcB. For LiH formation, it suggests partial dehydrogenation of $LiBH_4$ during nanoconfinement as reported in previous work (Gosalawit–Utke et al., 2014). Although the B_xO_y (x/y = 3) signals, corresponding to $LiBH_4$/PcB interaction, is observed in nano $LiBH_4$–PcB–MWCNT, the relative amount of B_xO_y (x/y = 3) with respect to $LiBH_4$ of nano $LiBH_4$–PcB–MWCNT is lower than that of nano $LiBH_4$–PcB. This results confirm that the interaction of $LiBH_4$/PcB is reduced by doping small amount of MWCNT in nano $LiBH_4$–PcB.

CHARPTER V

CONCLUSIONS

In this thesis, nanoconfined $LiBH_4$ in PcB–MWCNT composite was successfully prepared and named nano $LiBH_4$–PcB–MWCNT. Nano $LiBH_4$–PcB–MWCNT started to release hydrogen at 85 °C (~4 times lower than the desorption temperature of milled $LiBH_4$). As compared to nanoconfined sample without MWCNT, thermal stability of polymer matrix was significantly improved by MWCNT addition. For example, total amount of gases release from thermal degradation of PcB in nanoconfined samples was reduced by 55.3 % after doping with 0.1 wt. % of MWCNT. The reduction of $LiBH_4$/PcB interaction was confirmed by the ratio of B–H stretching peak area with respect to that of C=O stretching (υ(B–H)/υ(C=O)) from FT–IR spectra. It is found that υ(B–H)/υ(C=O) ratio significantly increases up to 78%. This is in agreement with B $1s$ XPS results, where the relative amount of B_xO_y (x/y=3) to $LiBH_4$ decreases after MWCNT doping. For dehydrogenation kinetics, comparable amounts of released H_2 were obtained from both nanoconfined samples in the 1st cycle, i.e., 6.7 and 6.6 wt. % H_2 with respect to $LiBH_4$ content from nano $LiBH_4$–PcB and nano $LiBH_4$–PcB–MWCNT, respectively. The slow kinetics observed in nano $LiBH_4$–PcB–MWCNT might be due to the random dispersion of MWCNT in PcB hindering the diffusion of H_2 in the polymer matrix. After rehydrogenation at 120 °C under 60 bar H_2, nano $LiBH_4$–PcB– MWCNT exhibited the amount of hydrogen reproducibility in the 2nd cycle of 37.3% with respect to theoretical hydrogen capacity, higher than that of nano $LiBH_4$–PcB (20.0%).
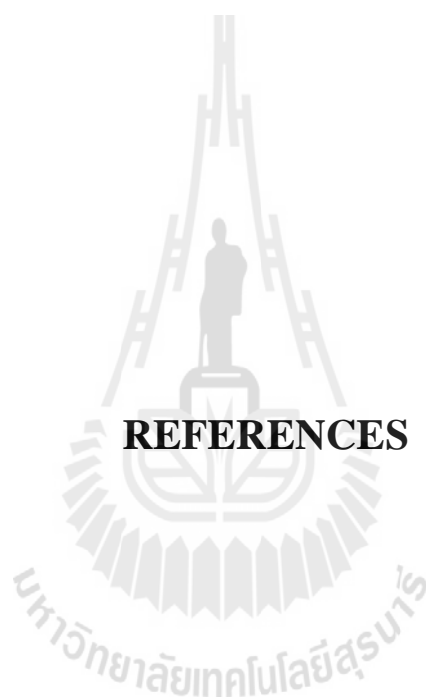
REFERENCES

REFERENCES

Au, M., Jurgensen, A. R., Spencer, W. A., Anton, D. L., Pinkerton, F. E., Hwang, S–J., Kim, C., and Bowman, R. C., Jr. (2008). Stability and reversibility of lithium borohydrides doped by metal halides and hydrides. **J. Phys. Chem. C**. 112: 18661–18671.

Bal, S. and Samal, S. S. (2007). Carbon nanotube reinforced polymer composite-A state of the art. **B. Mater. Sci.** 30: 379–386.

Checchetto, R., Bazzanella, N., Miotello, A., Carotenuto, G., and Nicolais, L. (2009). Hydrogen sorption in metal composites: the role of interfaces. **J. Appl. Phys.** 105: 083513.

Chipara, M., Villarreal, J. R., Chipara, M. D., Lozano, K., Chipara, A. C., and Sellmyer, D. J. (2009). Spectroscopic investigations on polypropylene–carbon nanofiber composites: *I. Raman and electron spin resonance spectroscopy.* **J. Polym. Sci. Phys.** 47:1644–1652.

Chipara, M. D., Macossay, J., Ybarra, A. V. R., Chipara, A. C., Eubanks, T. M., and Chipara, M. (2013). Raman spectroscopy of polystyrene nanofibers–Multiwalled carbon nanotubes composites. **Appl. Surf. Sci.** 275:23–27.

Deprez, E., Muñoz–Márquez, M. A., Jimenez de Haro, M. C., Palomares, F. J., Soria, F., Dornheim, M., Dornheim, M., Bormann, R., and Fernández1, A. (2011). Combined x−ray photoelectron spectroscopy and scanning electron microscopy studies of the. $LiBH_4−MgH_2$ reactive hydride composite with and without a Ti−based additive. **J Appl. Phys.** 109: 014913.

Fang, Z. Z., Wang, P., Rufford, T. E., Kang, X. D., Lu, G. Q., and Cheng, H. M. (2008). Kinetic and thermodynamic–based improvements of lithium borohydride incorporated in activated carbon, **Acta Mater.** 56: 6257−6263.

Fang, Z. Z., Kang, X. D., Yang, Z. X., Walker, G. S., and Wang, P. (2011). Combined effects of functional cation and anion on the reversible dehydrogenation of $LiBH_4$. **J. Phys. Chem. C.** 115: 11839−11845.

Friedrichs, O., Remhof, A., Hwang, S. J., and Züttel, A., (2010). Role of $Li_2B_{12}H_{12}$ for the formation and decomposition of $LiBH_4$, **Chem. Mater.** 22: 3265.

Gosalawit–Utke, R., Meethom, S., Pistidda, C., Milanese, C., Laipple, D., Saisopa, T.,Marini, A., Klassen, T., and Dormheim, M. (2014). Destabilization of $LiBH_4$ by nanoconfinement in PMMA–co–BM polymer matrix for reversible hydrogen storage. **Int. J. Hydrogen Energ.** 39: 5019–5029.

Gross, A. F., Vajo, J. J., Atta, S. L. V., and Olson, G. L. (2008). Enhanced hydrogen storage kinetics of $LiBH_4$ in nanoporous carbon scaffolds. **J. Phys. Chem. C.** 112: 5651−5657.

Guo, Y. H., Yu, X. B., Gao, L., Xia, G. L., Guo, Z. P., and Liu, H. K., (2010). Significantly improved dehydrogenation of $LiBH_4$ destabilized by TiF_3. **Energ. Environ. Sci.** 3: 465–470.

Harris, P. M. and Meibohm, E. P. (1947). The crystal structure of lithium borohydride ($LiBH_4$). **J. Am. Chem. Soc.** 69: 1231–1232.

Haipinga, W., Tiechengb, L., Xuemina, W., Fangfanga, G., Linhonga, C., Honglianga, Z., Chunhonga, L., Xiaohanc, Y., and Xind, J., and Weidong, W. (2011). Corrosion characteristics of $LiBH_4$ film exposed to a $CO_2/H_2O/O_2/N_2$ mixture. **Corros. Sci.** 53: 1115–1119.

Huang, J., Yan, Y., Ouyang, L., Wang, H., Liu, J., and Zhu, M. (2014). Increased air stability and decreased dehydrogenation temperature of $LiBH_4$ via modification within poly(methyl methacrylate). **Dalton. T.** 43: 410–413.

Ibikunle, A., Goudy, A. J., and Yang, H. (2009). Hydrogen storage in a CaH_2/ $LiBH_4$ destabilized metal hydride system, **J. Alloy Compd.** 475: 110–115.

Jeon, K. J., Moon, H. I., Ruminski, A. M., Jiang, B., Kisielowski, C., Bardhan, R., and Urban, J. J. (2011). Air–stable magnesium nanocomposites provide rapid and high–capacity hydrogen storage without using heavy–metal catalysts, **Nat. mater.** 10: 286–290.

Kang, X–D., Wang, P., Ma, L–P., and Cheng, H–M. (2007). Reversible hydrogen storage in $LiBH_4$ destabilized by milling with Al. **Appl. Phys. A.** 89: 963–966.

Kashiwagi, T., Inaba, A., Brown, J. E., Hatada, K., Kitayama, T., and Masuda, E. (1986). Effects of weak linkages on the thermal and oxidative degradation of poly(methyl methacrylates). **Macromolecules.**19: 2160–2168.

Kashiwagi, T., Inabi, A., and Hamins, A. (1989). Behavior of Primary Radicals during Thermal Degradation of Poly(methyl methacrylate). **Polym. Degrad. Stabil.** 26: 161–184.

Kashiwagi, T., Grulke, E., Hilding, J., Harris, R., Awad, W., and Douglas J. (2002). Thermal degradation and flammability properties of poly(propylene)/carbon nanotube composites. **Macromol. Rapid. Commun.** 23: 761–765.

Li, C., Peng, P., Zhou, D. W., and Wan L. (2011). Reshearch progress in $LiBH_4$ for hydrogen storage: A review. **Int. J. Hydrogen. Energ.** 36: 14512–14526.

Lim, J–H., Shim, J–H., Lee, Y–S., Suh, J–Y., Cho, Y. W., and Lee, J. (2010). Rehydrogenation and cycle studies of $LiBH_4$–CaH_2 composite. **Int. J. Hydrogen. Energ.** 35: 6578–6582.

Litster, S. and McLean, G. (2004). PEM fuel cell electrodes. **J. Power Sources.** 130: 61–71.

Liu, X., Peaslee, D., Jost, C. Z., and Majzoub, E. H. (2010). Controlling the decomposition pathway of $LiBH_4$ via confinement in highly ordered nanoporous carbon. **J. Phys. Chem. C.** 114: 14036–14041.

Liu, X., Peaslee, D., Jost, C. Z., Baumann, T. F., and Majzoub, E. H. (2011). Systematic pore-size effects of nanoconfinement of $LiBH_4$: elimination of diborane release and tunable behavior for hydrogen storage applications. **Chem. Mater.** 23: 1331– 1336.

Llamas–Jansa, I., Aliouane, N., Deledda, S., Fonneløp, J. E., Frommen, C., Lieutenant, K., Sartori, S., Sørby, M. H., and Hauback, B. C. (2011). Mechano–chemical reactions in $LiBH_4$ + VCl_n (n = 2 and 3) mixtures. **J. Alloy. Compd.** 509: S684–S687.

Mao, J. F., Guo, Z. P., Liu, H. K., and Yu, X. B. (2009). Reversible hydrogen storage in titanium–catalyzed $LiAlH_4$–$LiBH_4$ system. **J. Alloy. Compd.** 487: 434–438.

Matsushita, A., Ren, Y., Matsukawa, K., Inoue, H., Minami, Y., Noda, I., and Ozaki, Y. (2000). Two–dimensional Fourier–transform Raman and near–infrared correlation spectroscopy studies of poly(methyl methacrylate) blends: 1. Immiscible blends of poly(methyl methacrylate) and atactic polystyrene. **Vib. Spectrosc.** 24: 171–180.

Montone, A., Aurora, A., Gattia, M. D., and Antisari, M. V. (2012). Microstructural and Kinetic Evolution of Fe Doped MgH_2 during H_2 Cycling. **Catalysts.** 2: 400–411.

Namouchi, F., Smaoui, H., Fourat,i N., Zerrouki, C., Guermazi, H., and Bonnet, J. J. (2009). Investigation on electrical properties of thermally aged PMMA by combined use of FTIR and impedance spectroscopies. **J. Alloy. Compd.** 469: 197-202.

Ngene, P., Adelhelm, P., Beale, A. M., Jong, K. P., and Jongh, P. E. (2010). $LiBH_4$/ SBA–15 Nanocomposites prepared by melt infiltration under hydrogen pressure: synthesis and hydrogen sorption properties. **J. Phys. Chem. C.** 114: 6163–6168.

Ngene, P. (2012). **Nanoconfined alkali-metal borohydrides for reversible hydrogen storage.** Ridderprint BV, Enugu.

Orimo, S. I., Nakamori, Y., Kitahara, G., Miwa, K., Ohba, N., Towata, S., and Züttel, A. (2005). Dehydriding and rehydriding reactions of $LiBH_4$, **J. Alloy. Compd.** 427–430: 404–406.

Orimo, S. I., Nakamori, Y., Ohba, N., Miwa, K., Aoki, M., Towata, S. I., and Züttel, A. (2006). Experimental studies on intermediate compound of $LiBH_4$, **Appl. Phys. Lett.** 89: 021920.

Ozolins, V., Majzoub, E. H., and Wolverton, C. (2009). First–principal prediction of thermodynamically reversible hydrogen storage reaction in the Li–Mg–Ca–B–H system, **J. Am. Chem. Soc.** 131: 230–237.

Pendolino, F., Mauron, P., Borgschulte, A., and Züttel, A. (2009). Effect of boron on the activation energy of the decomposition of LiBH$_4$. **J. Phys. Chem. C.** 113: 17231–17234.

Pentimalli, M., Padella, F., Barbera, A. L., Pilloni, L., and Imperi, E. (2009). A metal hydride– polymer composite for hydrogen storage applications. **Energ. Convers. Manage.** 50: 3140–3146.

Pinkerton, F. E., Meisner, G. P., Meyer, M. S., Balogh, M. P., and Kundrat, M. D. (2005). Hydrogen desorption exceeding ten weight percent from the new quaternary hydride Li$_3$BN$_2$H$_8$. **J. Phys. Chem. B.** 109: 6–8.

Pinkerton, F.E. and Meyer, M.S., (2008). Reversible hydrogen storage in the lithium borohydrid–calcium hydride coupled system. **J. Alloy. Compd.** 464: L1–L4.

Principi, G., Agresti, F., Maddalena, A., and Russo, S. L. (2009). The problem of solid state hydrogen storage. **J. Energy.** 34: 2087–2091.

Ravnsbaek, D. B. and Jensen, T. R. (2010). Tuning hydrogen storage properties and reactivity: investigation of the LiBH$_4$–NaAlH$_4$ system. **J. Phys. Chem. Solids.** 71: 1144–1149.

Schlapbach, L. and Züttel, A. (2001). Review article Hydrogen-storage materials for mobile applications. **Nature.** 414: 353–358.

Schwartz, A. M. (1978). The benzophenone/ketyl tetrahydrofuran (THF) still. **Chem. Eng. News.** 56: 88.

Sun, T., Liu, J., Wang, H., Sun, D., Zhu, M., and Yao, X. (2012). Confined LiBH$_4$: Enabling fast hydrogen release at ~100 $^{\circ}$C. **Int. J. Hydrogen. Energ.** 37: 18920–18926.

Swain, S. K. and Jena, I. (2010). Polymer/carbon nanotube nanocomposites: A novel material. **Asian. J. Chem.** 22: 1–15.

Tollefson J. (2010). Fuel of the Future. **Nature**. 464: 1262–1264.

Vajo, J. J. and Skeith, S. L. (2005). Reversible storage of hydrogen in destabilized LiBH$_4$. **J. Phys. Chem. B.** 109: 3719–3722.

Varin, R. A., Czujko, T., and Wronski, Z. S. (2009). **Nanomaterials for Solid State Hydrogen Storage.** Springer, Cleveland.

Velasco-Santos, C., Martínez-Hernández, A. L., Fisher, F. T., Ruoff, R., and Castaño, V. M. (2003). Improvememt of thermal and mechanical properties of carbon nanotube composite through chemical functionalization. **Chem. Mater.** 15: 4470–4475.

Xia, G. L., Guo, Y. H., Wu, Z., Yu, and X. B. (2009). Enhanced hydrogen storage performance of LiBH$_4$–Ni composite. **J. Alloy. Compd.** 479: 545–548.

Yang, J., Sudik, A., and Wolverton, C. (2007). Destabilizing LiBH$_4$ with a Metal (M = Mg, Al, Ti, V, Cr, or Sc) or Metal Hydride (MH$_2$ = MgH$_2$, TiH$_2$, or CaH$_2$). **J. Phys. Chem. C.** 111: 19134–19140.

Yu, X. B., Grant, D. M., and Walker, G. S. (2008). Low–temperature dehydrogenation of LiBH$_4$ through destabilization with TiO$_2$. **J. Phys. Chem. C.** 112: 11059–11062.

Yu, X. B., Grant, D. M., and Walker, G. S. (2009). Dehydrogenation of LiBH$_4$ destabilized with various oxides. **J. Phys. Chem. C.** 113: 17945–17949.

Zhang B. J. and Liu B. H. (2010). Hydrogen desorption from LiBH$_4$ destabilized by chlorides of transition metal Fe, Co, and Ni. Int. J. Hydrogen. Energ. 35: 7288–7294.

Zhang, B. J., Liu, B. H., and Li, Z. P. (2010). Destabilization of LiBH$_4$ by (Ce, La) (Cl, F)$_3$ for hydrogen storage. **J. Alloy. Compd.** 509: 751–757.

Züttel, A., Wenger, P., Rentsch, S. Sudan, P., Mauron, P., and Emmenegger, C. (2003). LiBH$_4$ a new hydrogen storage material. **J. Power Sources.** 118: 1–7.

Züttel, A., Rentsch, S., Fischer, P., Wenger, P., Sudan, P., Mauron, P., and Emmenegger, C. (2003). Hydrogen storage properties of LiBH$_4$. **J. Alloy. Compd.** 356–357: 515–520.

Züttel, A., Borgschulte, A., and Schlapbach, L. (2008). **Hydrogen as a future energy carrier.** Wiley-VCH, Weinheim.

APPENDICES
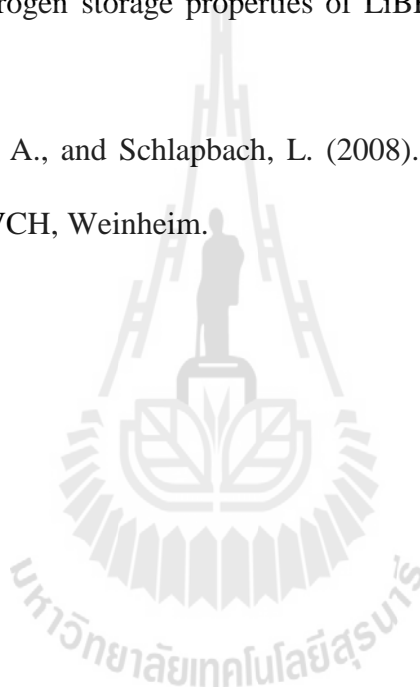
APPENDIX A

HYDROGEN STORAGE CAPACITY OF MATERIALS

A.1 Calculation of theoretical hydrogen storage capacity of samples

- **Amount of LiBH₄ in samples**

  - Molecular weight of $LiBH_4$ = 22 g/mol

  - Pipet 10.00 mL of 2.0 M of $LiBH_4$

    $\therefore$ Amount of LiBH₄ in samples $= \left(\dfrac{(2.0 \text{ M}) \times (10.00 \text{ mL})}{1000}\right) \times 22 \text{ g/mol}$

    $= \quad 0.44$ g

- **Nanoconfined LiBH₄ in PMMA-co-BM (LiBH₄-PcB)**

From amount of PMMA−co−BM (5.0565 g) and LiBH₄ (0.66 g), wt. % of LiBH₄ in PMMA−co−BM is calculated by:

$\quad$ Wt. % of LiBH₄ in sample $\quad = \quad \left(\dfrac{0.66 \text{ g}}{5.0565 \text{ g} + 0.66 \text{ g}}\right) \times 100$

$\quad\quad\quad\quad\quad\quad\quad\quad\quad\quad\quad = \quad 11.5$ wt. %

Based on 13.6 wt. % of H₂ released by pure LiBH₄, the theoretical of hydrogen capacity of LiBH₄–PcB is calculated by:

$\quad\quad$ Wt. % of H₂ $\quad = \quad \dfrac{(13.6 \times 11.5)}{100}$

$\quad\quad\quad\quad\quad\quad\quad = \quad 1.6$ wt. % H₂

- **Nanoconfined LiBH₄ in PMMA-co-BM-MWCNT composite (LiBH₄-PcB-MWCNT)**

From amount of PMMA−co−BM (5.0745 g), MWCNT (0.0055 g) and LiBH₄ (0.44 g), wt. % of LiBH₄ in PMMA−co−BM is calculated by:

$$\text{Wt. \% of LiBH}_4 \text{ in sample} \quad = \quad \left(\frac{0.44\ \text{g}}{5.0745\ \text{g} + 0.0055\ \text{g} + 0.44\ \text{g}}\right) \times 100$$

$$= \quad 8.0\ \text{wt. \%}$$

Based on 13.6 wt. % of H₂ released by pure LiBH₄, the theoretical of hydrogen capacity of LiBH₄–PcB is calculated by:

$$\text{Wt. \% of H}_2 \quad = \quad \frac{(13.6 \times 8.0)}{100}$$

$$= \quad 1.1\ \text{wt. \% H}_2$$

A.2 Calculation of hydrogen desorption capacity

- **Theory**

The amount of hydrogen release from samples will be calculated based on the amount of LiBH₄ in the sample by using the ideal gas law (Varin et al., 2009):

$$PV \quad = \quad nRT \qquad\qquad (1)$$

where, P is gas pressure (atm), V is gas volume (L), n is number of moles of gas (mole), T is absolute temperature of gas (K), and R is the universal gas constant (0.08206 L· atm · mol⁻¹ · K⁻¹).

The relation between hydrogen pressure in the system and a number of hydrogen moles at temperature (T) prior to de/rehydrogenation can be described by:

$$P_1V \quad = \quad n_1RT \qquad \qquad (2)$$

After de/rehydrogenation, new values of hydrogen pressure and moles are as followed:

$$P_2V \quad = \quad n_2RT \qquad \qquad (3)$$

where, $P_1 > P_2$ for rehydrogenation and $P_1 < P_2$ for dehydrogenation.

Therefore, the difference between number of hydrogen moles resulting from rehydrogenation or dehydrogenation is calculated by the following equation:

$$\Delta n \ = \ n_1 \ - \ n_2 \quad = \quad \Delta P \frac{V}{RT} \qquad \qquad (4)$$

Where, $\Delta P = P_1 - P_2$.

The mass of absorbed or desorbed hydrogen can be calculated from the number of moles of gas and molecular mass of hydrogen:

$$M_{H_2} \quad = \quad 2.016 \ \Delta P \frac{V}{RT} \qquad \qquad (5)$$

When the hydrogen mass is known using equation (6). The hydrogen capacity (wt. %) of the investigated materials can be calculated by:

$$\text{Hydrogen capacity (wt. \%)} \quad = \quad \frac{M_{H_2}}{\text{Mass of sample}} \ \times \ 100 \qquad \qquad (6)$$

- **Amount of desorbed H_2 of LiBH$_4$-PcB**

  - 1st dehydrogenation cycle

    $P_1 = \quad$ -0.60 atm $\qquad \qquad P_2 = $ -1.33 atm

    $T = \quad$ 120 °C $\qquad \qquad V = 0.0240$ L

    $R = 0.08206$ L·atm·K^{-1}·mol^{-1} $\qquad$ Sample weight = 0.1402 g

    $$M_{H_2} \quad = \quad 2.016 \times (-1.33 - (-0.60)) \frac{0.0240}{(0.08206 \times (120 + 273))}$$

    $$= \quad 5.51 \times 10^{-4} \text{ g}$$

$$\text{Hydrogen capacity (wt. \%)} \quad = \quad \frac{5.51 \times 10^{-4} \text{ g}}{0.1402 \text{ g}} \quad \times \quad 100$$

$$= \quad 0.78 \text{ wt. \%}$$

- 2nd dehydrogenation cycle

$P_1 =$ -1.33 atm $\qquad\qquad$ $P_2 =$ -1.04 atm

$T =$ 120 °C $\qquad\qquad\qquad$ $V =$ 0.0240 L

$R = 0.08206 \text{ L·atm·K}^{-1}\text{·mol}^{-1}$ $\qquad$ Sample weight = 0.1402 g

$$M_{H_2} \quad = \quad 2.016 \times (-1.04 - (-1.33)) \frac{0.0240}{(0.08206 \times (120 + 273))}$$

$$= \quad 4.35 \times 10^{-4} \text{ g}$$

$$\text{Hydrogen capacity (wt. \%)} \quad = \quad \frac{4.35 \times 10^{-4} \text{ g}}{0.1402 \text{ g}} \quad \times \quad 100$$

$$= \quad 0.31 \text{ wt. \%}$$

- **Amount of desorbed H$_2$ of LiBH$_4$-PcB-MWCNT**

  - 1st dehydrogenation cycle

$P_1 =$ 0.00 atm $\qquad\qquad$ $P_2 = 0.412$ atm

$T =$ 120 °C $\qquad\qquad\qquad$ $V = 0.0213$ L

$R = 0.08206 \text{ L·atm·K}^{-1}\text{·mol}^{-1}$ $\qquad$ Sample weight = 0.1030 g

$$M_{H_2} \quad = \quad 2.016 \times (0.412 - 0) \frac{0.0213}{(0.08206 \times (120 + 273))}$$

$$= \quad 5.48 \times 10^{-4} \text{ g}$$

$$\text{Hydrogen capacity (wt.\%)} \quad = \quad \frac{5.48 \times 10^{-4} \text{ g}}{0.1030 \text{ g}} \quad \times \quad 100$$

$$= \quad 0.53 \text{ wt. \%}$$

- 2nd dehydrogenation cycle

$P_1 =$ 0.00 atm $\qquad\qquad$ $P_2 =$ 0.32 atm

$T =$ 120 °C $\qquad\qquad$ $V =$ 0.0213 L

$R = 0.08206 \text{ L} \cdot \text{atm} \cdot \text{K}^{-1} \cdot \text{mol}^{-1}$ $\qquad$ Sample weight = 0.1030 g

$$M_{H_2} \quad = \quad 2.016 \times (0.32 - 0) \frac{0.0213}{(0.08206 \times (120 + 273))}$$

$$= \quad 4.26 \times 10^{-4} \text{ g}$$

$$\text{Hydrogen capacity (wt.\%)} \quad = \quad \frac{4.26 \times 10^{-4} \text{ g}}{0.1030 \text{ g}} \quad \times \quad 100$$

$$= \quad 0.41 \text{ wt. \%}$$

APPENDIX B

THESIS OUTPUT

1. Plerdsranoy, P., Wiset, N., Minalese, C., Laipple, D., Marini, A., Klassen, T., Dornheim, M., and Gosalawit–Utke, R. (2015). Improvement of thermal stability and reduction of $LiBH_4$/polymer host interaction of nanoconfined $LiBH_4$ for reversible hydrogen storage **Int. J. Hydrogen. Energ.** 40: 392–402.

CURRICULUM VITAE

Name   Miss Praphatsorn   Plerdsranoy

Date of Birth   30 August 1988

Address   26 Moo 11, Toom Sub district, Pakthongchai District, Nakhon
                     Ratchasima 30150, Thailand

Education

2007–2010   B.Sc. (Chemistry), Rajamankala University of Technology Isan,
                      Thailand

2011–present   Student in M.Sc. Program in Chemistry, Suranaree University of
                      Technology, Thailand

Research presentation:

Plerdsranoy P., Gosalawit–Utke R., Minalese C., Laipple D., Marini A., Klassen T., Dornheim M. "Nanodispersed $LiBH_4$ in PMMA/MWCNT composite for reversible hydrogen storage", Pure and Applied Chemistry International Conference 2014, Khon Kaen, Thailand, January 8 – 10. (Oral presentation).